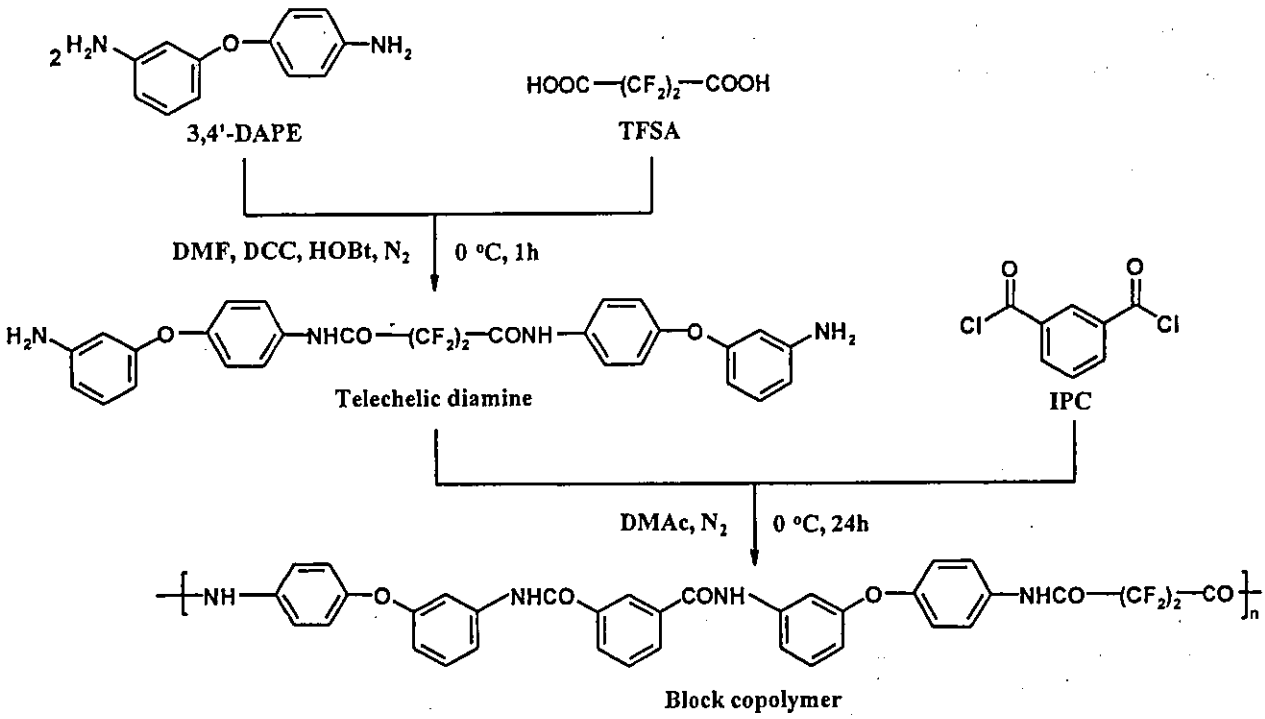

Scheme 1. Synthesis of the fluoroethylene–aramid block copolymer.

at 0 °C under a nitrogen atmosphere. Dicyclohexylurea was removed by filtration. After filtration, 60 mL of ethyl acetate was added to the filtrate. The organic layer was washed with a saturated sodium bicarbonate solution (30 mL × 3) and brine (30 mL × 3) and was dried over anhydrous sodium sulfate. After filtration, the filtrate was concentrated *in vacuo*. The crude product was purified with silica gel column chromatography (Merck Silica Gel 60, 230–400 mesh) eluting with chloroform/methanol (9.5:0.5 v/v) to give the telechelic diamine as a white solid.

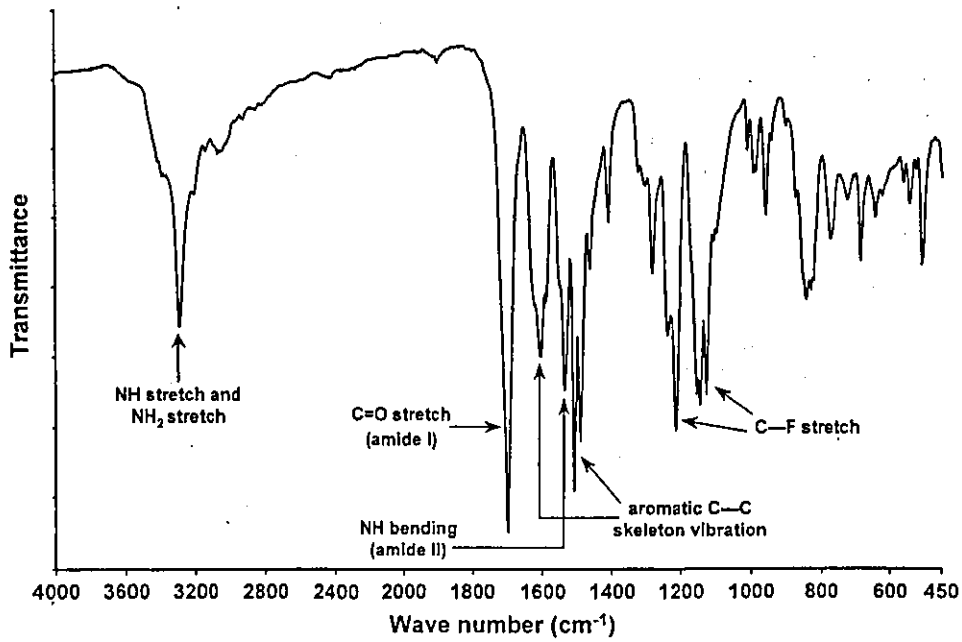

Figure 1. IR spectrum of the telechelic diamine containing a fluoroethylene segment.

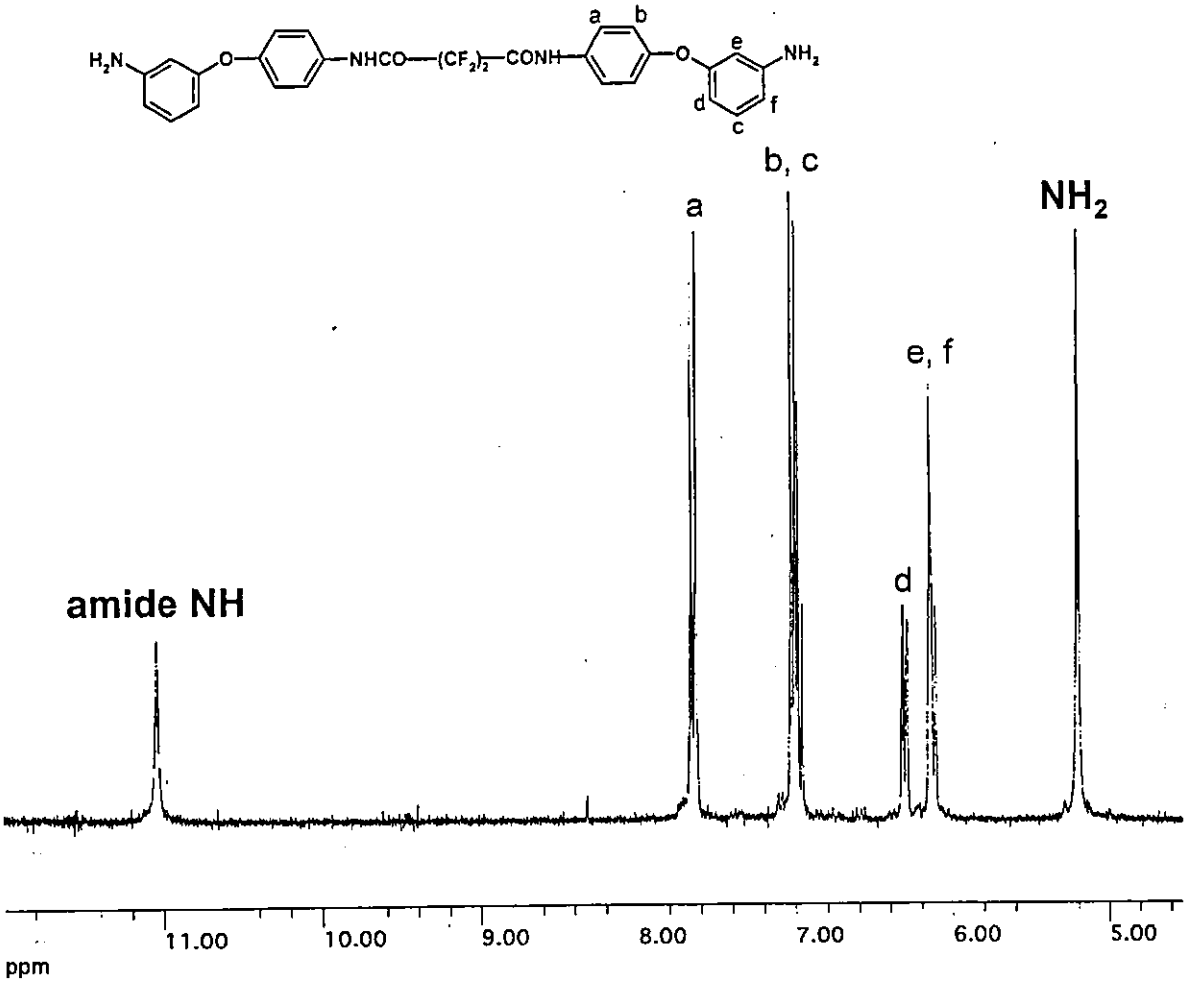

Figure 2. ^{1}H NMR spectrum of the telechelic diamine containing a fluoroethylene segment.

Synthesis of the Fluoroethylene–Aramid Block Copolymer

The telechelic diamine (0.80 g, 1.44 mmol) and 1.5 mL of anhydrous *N,N'*-dimethylacetamide (DMAc) were placed in a thoroughly dried, 100-mL, three-necked, round-bottom flask equipped with a mechanical stirrer under a nitrogen atmosphere. After the solution was cooled with an ice bath, 0.29 g (1.44 mmol) of isophthaloyl chloride (IPC) in anhydrous DMAc (1.5 mL) was added slowly to the stirred solution. The reaction mixture was maintained at 0 °C and stirred for 24 h under a nitrogen atmosphere. The copolymer was precipitated by the pouring of the reaction mixture into excess isopropyl alcohol with stirring and was purified by reprecipitation with hot DMAc/isopropyl alcohol.

Measurements

IR spectra were recorded on a Spectrum One Fourier transform infrared spectrometer (PerkinElmer, MA), and ^{1}H NMR spectra were recorded on a Gemini 300 spectrometer (Varian, Inc., CA) with tetramethylsilane as an internal standard. The molecular weight and molecular weight distribution were determined with an HLC8220 GPC instrument (Tosoh Co., Ltd., Tokyo, Japan) with TSKgel Super AW4000 and Super AW3000 columns in DMF (with polystyrene standards, a column temperature of 40 °C, and DMF as an eluent with 10 mmol/L of LiBr).

RESULTS AND DISCUSSION

Before the synthesis of the telechelic diamine and the block copolymer in Scheme 1, the synthetic method of Imai et al.[10] was attempted as follows. The aramid oligomer was prepared by the reaction of 3,4'-DAPE with IPC in the first step, and the block copolymer was synthesized by direct polycondensation between the aramid oligomer and TFSA in the second step. However, the fluorinated block copolymer could not be ob-

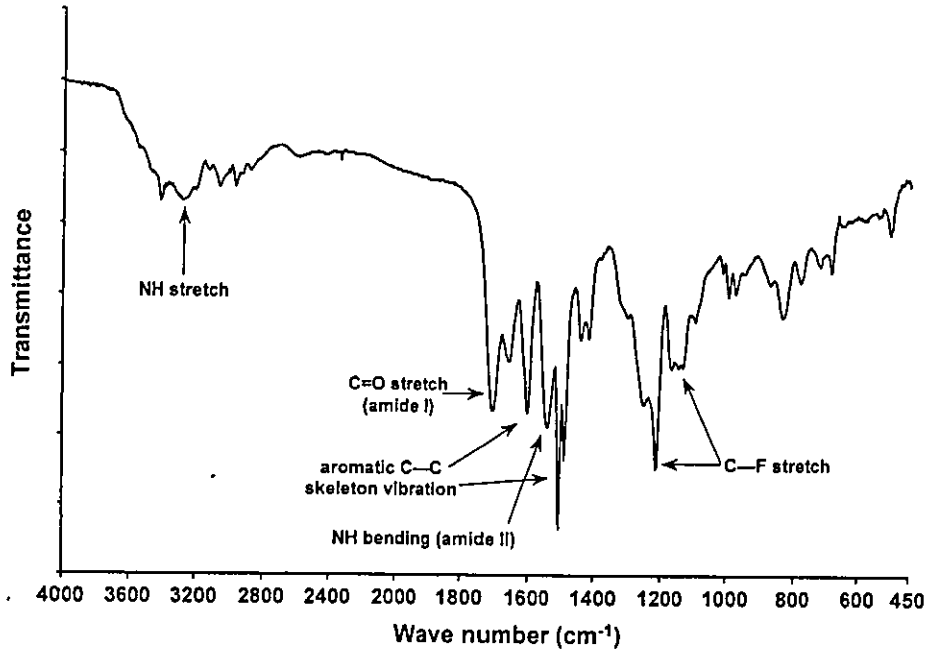

Figure 3. IR spectrum of the block copolymer.

tained in this way, and this can be explained by the assumption that the aramid segment develops a high molecular weight easily because of the low probability of the reaction between the amine groups of the aramid oligomer and the carboxylic groups of TFSA. The other synthetic way, shown in Scheme 1, was then attempted. The telechelic diamine was prepared by the reaction of TFSA with 3,4′-DAPE in anhydrous DMF in the presence of DCC in the first step. Because the molecular weights of the telechelic diamine and IPC were small, the reaction between the amine groups of the telechelic diamine and the carboxylic groups of IPC was easily carried out. In view of the solubility parameter, the telechelic diamine and IPC, moreover, could be reacted easily. The solubility parameter of the telechelic diamine was calculated to be 13.2 with a group contribution calculation.[11] This value was close to those of IPC and DMAc (11.7 and 10.8, respectively). In the second step in Scheme 1, the telechelic diamine and IPC were mixed homogenously, and this made it possible to synthesize the block copolymer.

In the first step, the telechelic diamine was prepared in the presence of HOBt as the additive. The purpose of the addition of HOBt in the synthesis of the telechelic diamine was to prohibit the formation of *N*-acylurea, a byproduct of the DCC coupling reaction, and to afford the telechelic diamine in a good yield and a high state of purity.[12–14] The yield of the telechelic diamine synthesized according to Scheme 1 without HOBt was 9.0%, but the yield of that synthesized according to Scheme 1 with HOBt was 17.6%.

The characterization of the telechelic diamine was based on its IR and ^{1}H NMR spectral data. Figure 1 shows the IR spectrum of the telechelic diamine. This spectrum shows the absorption bands due to NH and NH_2 stretching at 3294, amide bonds at 1699 (C=O stretching, amide I) and 1535 (NH bending, amide II), aromatic C—C stretching at 1604, 1506, and 1489, and C—F stretching at 1216 and 1147 cm^{-1}. Figure 2 shows the ^{1}H NMR spectrum of the telechelic diamine. The singlet at 5.20 ppm is attributed to the terminal NH_2 groups, whereas the singlet at 11.06 ppm is attributed to the amide bond NH. The peak of the amide bond of the telechelic diamine shifts to the low magnetic field side with respect to that of a conventional aramid.[15] This is due to the presence of CF_2. The electronegativity of fluorine is higher than that of carbon (4.0 and 2.5, respectively). Therefore, the proton of the amide bond neighbor to CF_2 is deshielded.[16] The peaks at 6.14–7.66 ppm are characteristic of the protons of the phenyl groups. From the peak position and the integrated value of these peaks, it is shown that carboxyl groups of TFSA react only with the amine groups of the para position of 3,4′-DAPE. It is presumed that this regioselectivity might be due to two factors: the steric hindrance of the active intermediate from the reaction of HOBt with TFSA and the difference in the reactivity of the phenyl substituent.[17]

The fluoroethylene–aramid block copolymer was obtained by the low-temperature solution polycondensation of the telechelic diamine with IPC in anhydrous DMAc. The polymer was obtained in a 76.1% yield as a white solid. The characterization of the block copolymer was based on its IR and ^{1}H NMR spectral data. Figure 3 shows the IR spectrum of the block copolymer. This spectrum shows the absorption bands due to NH

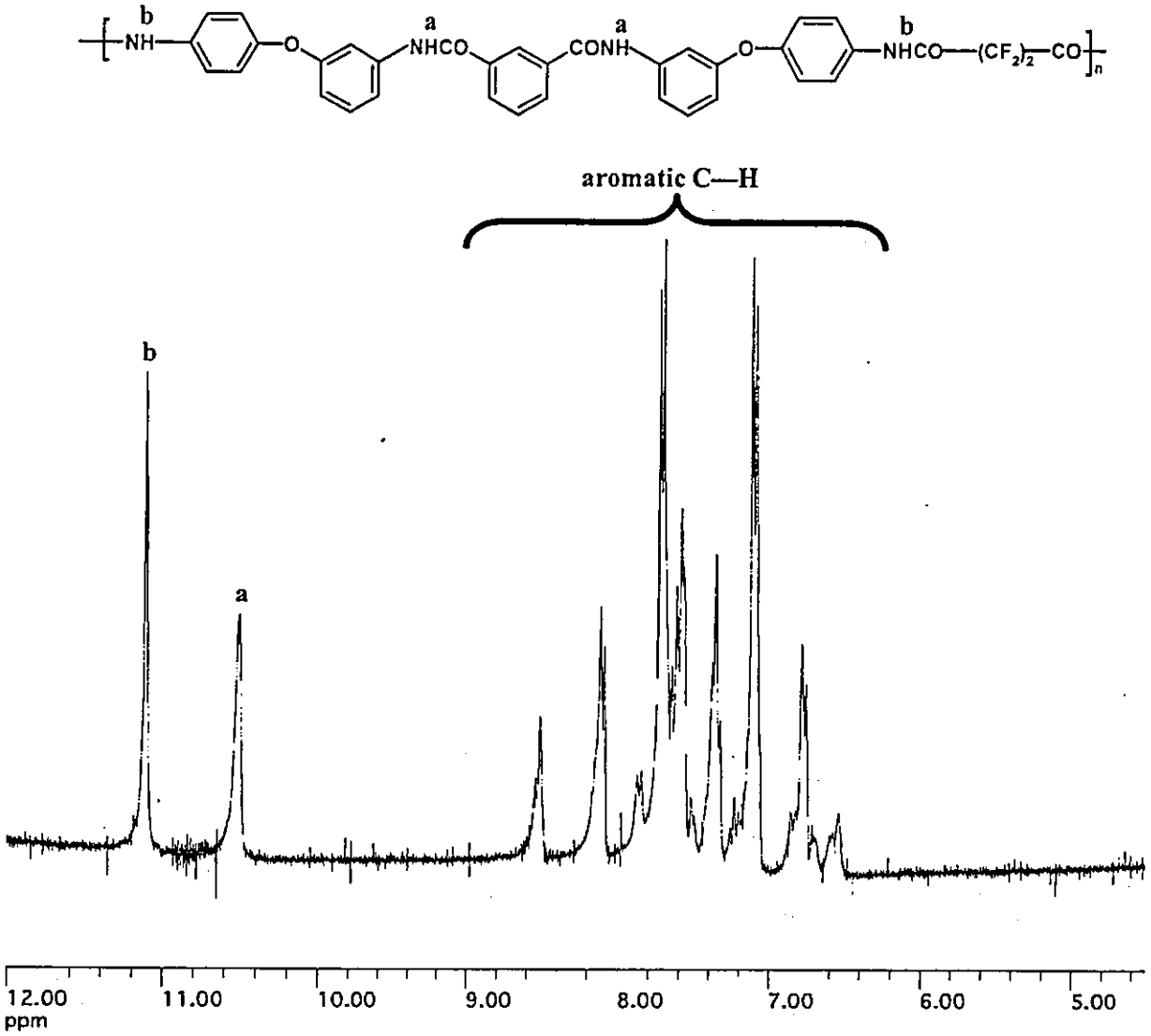

Figure 4. ^{1}H NMR spectrum of the block copolymer.

stretching at 3277, amide bonds at 1707 (C=O stretching, amide I) and 1538 (NH bending, amide II), aromatic C—C stretching at 1601, 1505, and 1487, and C—F stretching at 1213 and 1167 cm^{-1}. Figure 4 shows the ^{1}H NMR spectrum of the block copolymer. The multiplet at 6.49–8.50 ppm belongs to aromatic C—H. The singlet at 10.51 ppm is attributed to the amide bonds of the aramid segments, and the singlet at 11.12 ppm is attributed to the amide bonds between the fluorocarbon and benzene rings. The disappearance of the singlet at 5.20 ppm observed in the ^{1}H NMR spectrum of the telechelic diamine proves that the terminal NH_2 groups of the diamine react completely with the acid chloride groups of IPC. In addition, the peak of the amide bonds between the fluorocarbon and benzene rings shifts to the low magnetic field side in agreement with the telechelic diamine. The amide bonds of the aramid segments, however, are not influenced by the fluorocarbon.

The molecular weight of the fluoroethylene–aramid block copolymer was investigated with GPC. The chromatogram of the block copolymer was monomodal. The number-average molecular weight was 17,200. The weight-average molecular weight was 27,500. The molecular weight distribution (weight-average molecular weight/number-average molecular weight) was 1.60. In view of the number-average molecular weight, this value shows that one molecule of the block copolymer consisted of about 25.1 repeating units.

Generally, aramids have poor solubility because of the high crystallinity and stiffness of the polymer backbones. For example, an aramid consisting of 3,4′-DAPE and IPC dissolves in polar solvents, such as DMAc and DMF, but not in acetone and tetrahydrofuran

(THF).[18,19] Many studies have focused on the solution of this problem.[20–25] As one of the solutions to this problem, the introduction of the fluorine-containing component to the aramid has been designed.[19,26–30] Our block copolymer was actually dissolved in acetone and THF in addition to polar solvents. This solubility of our block copolymer in the solvents is similar to that of the fluorine-containing aromatic polyamides in previous studies because the fluorine atom has weak intermolecular cohesive energy.[27,31] This result proves that incorporating fluoroethylene segments improves the solubility of the resulting polymer.

The block copolymer (10 w/v % THF solution) was cast onto a glass plate and dried at room temperature for 24 h. The film made by this casting method was slightly yellowish and transparent, and its surface was flat and smooth.

CONCLUSIONS

The telechelic diamine was synthesized by condensation with 3,4'-DAPE and TFSA in dry DMF in the presence of DCC and HOBt as condensing agents, and the fluoroethylene–aramid block copolymer was synthesized by polycondensation in anhydrous DMAc with the telechelic diamine and IPC. In contrast, polycondensation between the aramid oligomer prepared previously and TFSA was not successful because the aramid oligomer developed a high molecular weight easily. The telechelic diamine and the block copolymer were characterized by IR and ^{1}H NMR. The number-average molecular weight investigated by GPC was over 1.7×10^4. Incorporating fluoroethylene segments improved the solubility of the resulting polymer. A further study of the synthesis of block copolymers with extended fluorocarbon chains and better mechanical and surface properties is in progress for the purpose of developing a novel biomaterial.

This study was financially supported in part by a Grant-in-Aid for Scientific Research (13480300) from the Japanese Ministry of Education, Culture, Sports, Science, and Technology.

REFERENCES AND NOTES

1. Okano, T.; Katayama, M.; Shinohara, I. J Appl Polym Sci 1978, 22, 369.
2. Boretos, J. W.; Detmer, D. E.; Donachy, J. H. J Biomed Mater Res 1971, 5, 373.
3. Takahara, A.; Tashita, J.; Kajiyama, T.; Takayanagi, M.; MacKnight, W. J. Polymer 1985, 26, 987.
4. Lyman, D. J.; Knutson, K.; McNeil, B.; Shibatani, K. Trans Am Soc Artif Intern Organs 1975, 21, 49.
5. Furuzono, T.; Yashima, E.; Kishida, A.; Maruyama, I.; Matsumoto, T.; Akashi, M. J Biomater Sci Polym Ed 1993, 5, 89.
6. Scheirs, J. Modern Fluoropolymers; Wiley: New York, 1997.
7. Hougham, G.; Johns, K.; Cassidy, P. E. Fluoropolymers: Synthesis and Properties; Plenum: New York, 1999.
8. Améduri, B.; Boutevin, B.; Kostov, G. Prog Polym Sci 2001, 105, 105.
9. Lin, J.; Sherrington, D. C. Adv Polym Sci 1994, 111, 179.
10. Kajiyama, M.; Kakimoto, M.; Imai, Y. Macromolecules 1989, 22, 4143.
11. Fedors, R. F. Polym Eng Sci 1974, 14, 147.
12. König, W.; Geiger, R. Chem Ber 1970, 103, 788.
13. König, W.; Geiger, R. Chem Ber 1970, 103, 2024.
14. König, W.; Geiger, R. Chem Ber 1970, 103, 2034.
15. Gan, L. H.; Blais, P.; Carlsson, D. J.; Suprunchuk, T.; Wiles, D. M. J Appl Polym Sci 1975, 19, 69.
16. Silverstein, R. M.; Webster, F. X. Spectrometric Identification of Organic Compounds, 6th ed.; Wiley: New York, 1998.
17. Jadhav, J. Y.; Preston, J.; Krigbaum, W. R. J Polym Sci Part A: Polym Chem 1989, 27, 1175.
18. Imai, Y.; Kajiyama, M.; Ogata, S.; Kakimoto, M. J Polym Sci Polym Chem Ed 1984, 22, 3183.
19. Kajiyama, M.; Kudo, J.; Mizumachi, H. J Polym Sci Part A: Polym Chem 1999, 37, 1135.
20. Lozano, A. E.; de Abajo, J.; de la Campa, J. G.; Preston, J. J Polym Sci Part A: Polym Chem 1992, 30, 1327.
21. Spiliopoulos, I. K.; Mikroyannidis, J. A.; Tsivgoulis, G. M. Macromolecules 1998, 31, 522.
22. Liaw, D. J.; Liaw, B. Y.; Yang, C. M.; Hsu, P. N.; Hwang, C. Y. J Polym Sci Part A: Polym Chem 2001, 39, 1156.
23. Jeong, H. J.; Kakimoto, M.; Imai, Y. J Polym Sci Part A: Polym Chem 1991, 29, 767.
24. Jeong, H. J.; Oishi,, Y.; Kakimoto, M.; Imai, Y. J Polym Sci Part A: Polym Chem 1990, 28, 3293.
25. Imai, Y.; Malder, N. N.; Kakimoto, M. J Polym Sci Polym Chem Ed 1985, 23, 797.
26. Caporiccio, G.; Strepparola, E.; Bargigia, G.; Novaira, G.; Peveri, G. Makromol Chem 1983, 184, 935.
27. Kiyotsukuri, T.; Tsutsumi, N.; Okada, K.; Asai, K.; Nagata, M. J Polym Sci Part A: Polym Chem 1988, 26, 2225.
28. Oishi, Y.; Harada, S.; Kakimoto, M.; Imai, Y. J Polym Sci Part A: Polym Chem 1989, 27, 3393.
29. Wang, C. S.; Yang, R. W. Polymer 1997, 38, 6109.
30. Schneider, H. A.; Steinhauser, N.; Mülhaupt, R. Polym Bull 1994, 32, 339.
31. Kiyotsukuri, T.; Nagata, M.; Nakashita, K.; Ishii, T. Sen-i Gakkaishi 1984, 40, T-381.

JOURNAL OF MATERIALS SCIENCE: MATERIALS IN MEDICINE 14 (2003) 973–978

Surface modification of a porous hydroxyapatite to promote bonded polymer coatings

ATSUSHI MATSUDA[1]*, TSUTOMU FURUZONO[2], DOMINIC WALSH[3], AKIO KISHIDA[2], JUNZO TANAKA[1]
[1]*Biomaterials Center, National Institute for Materials Science, 1-1 Namiki, Tsukuba, Ibaraki 305-0044, Japan*
[2]*Department of Bioengineering, National Cardiovascular Center Research Institute, 5-7-1 Fujishiro-dai, Suita, Osaka 565-8565, Japan*
[3]*School of Chemistry, University of Bristol, Cantock Close, Bristol BS8 1TS, UK*
Email: Matsuda.atsushi@nims.go.jp

Porous hydroxyapatite (Hap) blocks were sintered at several temperatures and methyl methacrylate (MMA) grafted onto the surface in a 2-step heterogeneous system as a model example for surface modification. First, sintered porous Hap was modified with 2-methacryloyloxyethylene isocyanate (MOI) monomer in anhydrous dimethyl sulfoxide using di-*n*-butyltin (IV) dilaurate as a catalyst and hydroquinone as an inhibitor. Amount of the introduction of MOI monomer on porous Hap was 1.62 wt% at sintered temperature 800 °C, 0.68 wt% at it of 1000 °C, and 0.59 wt% at it of 1200 °C. Scanning electron microscopy (SEM) showed that porous Hap pore size and shape before and after MOI treatment were unchanged. Second, graft polymerization with MMA through the vinyl bond on porous Hap was conducted using α,α′-azobis isobutyronitrile (AIBN) as an initiator. Amount of Grafted PMMA on the MOI modified porous Hap was 2.84 wt% at sintered temperature of 800 °C, 6.97 wt% at it of 1000 °C, and 6.27 wt% at it of 1200 °C. MOI-modified and PMMA-grafted porous Hap were characterized using Fourier transform infrared (FT-IR) spectroscopy. The compressive strength of sintered porous Hap with grafted PMMA increased about 2.7–6.7 times compared to intact porous Hap. This 2-step surface modification on porous Hap is widely applicable to graft polymerization with vinyl polymer and conjugation with a protein or an oligopeptide, such as growth factor or an adhesion molecule, to improve Hap mechanical properties and functionality.

1. Introduction

Hydroxyapatite (Hap) has been used in medical applications such as bone implant materials [1–3]. Porous natural corals have also been used because the macroporosity of these materials promotes osteoconductivity and resorption *in vivo*. Walsh *et al.* reported synthesizing unique porous Hap with continuous cavities formed by a foaming calcium phosphate preparation [4, 5]. Porous Hap was applicable for graft cartridges in maxillofacial surgery [6] as alveolar ridge augments and as bone defect filler [7]. Mechanical strength, or cell adhesion and tissue migration on porous Hap, may be limited by its crystallinity, or surface composition and morphology [8–12]. The use of Hap in medical implants would greatly increase if surface modification by an organic compound could improve its mechanical strength or functionality of cell adhesion or multiplication.

Composite preparation of organic materials with Hap has involved the use of coupling agents, such as silanes [13–15], zirconyl salts [16], and polyacid [17], and the introduction of a chemical linkage to octacalcium phosphate by coprecipitation [18, 19]. As is well known, organic compounds with isocyanate groups react readily with Hap surface hydroxyl groups [20].

This paper details a novel 2-step surface modification with an organic compound that improves porous Hap mechanical properties and functionality. We chose poly methyl methacrylate (PMMA) as a typical example for porous Hap surface modification. PMMA is a common polymer used as bone cement for fixing total hip prostheses [15, 18, 19, 21] to give suitable mechanical properties to the material. Initially, 2-methacryloyloxyethylene isocyanate (MOI) possessing a vinyl polymerizable double bond and a reactive isocyanate group at both ends of the compound is reacted with a hydroxyl group of Hap to introduce vinyl groups, applicable as initiation points for grafting PMMA onto porous Hap. We then studied reaction kinetics and the effect on porous Hap shape and microstructure.

*Author to whom all correspondence should be addressed.

0957–4530

2. Materials and methods

2.1. Materials

The following were used without further purification: calcium hydrogen phosphate dihydrate ($CaHPO_4 \cdot 2H_2O$) and calcium bis(dihydrogen phosphate) monohydrate ($Ca(H_2PO_4)_2 \cdot H_2O$, MCPM) (Wako Pure Chemical Industries, Ltd., Osaka, Japan); calcium carbonate ($CaCO_3$) (Kanto Chemical Co., Inc., Tokyo, Japan); and MOI monomer donated by Showa Denko Co. (Tokyo, Japan). The solvent dimethyl sulfoxide dehydrate (DMSO), the catalyst di-*n*-butyltin (IV) dilaurate, the inhibitor hydroquinone, and the solvent *N*,*N*′-dimethyl formamide dehydrate (DMF) were purchased from Wako Pure Chemical Industries, Ltd. Methyl methacrylate (MMA) was purchased from Wako Pure Chemical Industries, Ltd., and distilled in a vacuum. The initiator α,α′-azobis isobutyronitrile (AIBN) was purchased from Wako Pure Chemical Industries, Ltd., and recrystallized from ethanol.

2.2. Measurements

Porous Hap was characterized by X-ray diffraction (XRD) (Philips PW1729 X-ray diffractometer, The Netherlands) with Ni-filtered Cu Kα radiation (40 kV, 50 mA). JCPDS-PDF card 9-432 was used for XRD reference. We used scanning electron microscopy (SEM, Model EDSEM, JEOL, Tokyo, Japan) at 10 kV acceleration voltage to observe tungsten-coated samples of intact porous Hap and its MOI composites. Infrared spectra (Perkin-Elmer FT-IR Spectrometer Spectrum 2000, USA) were recorded from 4000–500 cm^{-1} using KBr discs. The amount of MOI and grafted PMMA on porous Hap was determined using thermogravimetry-differential thermal analysis (TG-DTA Rigaku Thermo plus TG8120, Japan). About 10 mg of samples were heated to 1200 °C at the heating rate of 20 °C/min. Compressive strength (Texture Analyzer Stable Micro Systems® TA-XT2i, UK) was measured on 10 mm × 20 mm cylindrical blocks (5) of intact porous Hap and PMMA-grafted porous Hap. Titration was used to determine the amount of MOI added to porous Hap samples as described elsewhere [24–26].

2.3. Chemical modification by MOI monomer

Porous Hap was prepared using a modification of that reported by Walsh *et al.* [4,5]. Briefly, equimolar tetracalcium phosphate monoxide ($Ca_4(PO_4)_2O$, TCPM), $CaCO_3$, and MCPM were thoroughly mixed and 0.01 N HCl aqueous solution was added to 1 ml against 1 mg of mixed powder. The effervescing mixture was then rapidly mixed in a pestle and mortar before being packed into cylindrical molds. The porous cement block was then dried at room temperature for 24 h before soaking in 10^{-5} N NaOH aqueous solution at 37 °C for 3 days followed by air drying. A porous Hap cylindrical block 10 mm × 20 mm was prepared to cut the cylinders and modified with MOI monomer in a heterogeneous system. Porous Hap was dried for 24 h at 120 °C before use. We immersed 20 pieces of dried porous Hap in 49 ml anhydrous DMSO under nitrogen, and added 1.5 ml of MOI monomer and 0.05 g of di-*n*-butyltin (IV) dilaurate to an anhydrous system containing 150 ppm of hydroquinone. The reaction system was kept at 60 °C for 3, 6, 12, and 24 h. Chemically modified porous Hap was successively washed with DMSO and methanol to remove unreacted reagents. MOI-modified samples were dried at room temperature in a vacuum oven for 24 h.

2.4. Graft polymerization with PMMA

PMMA was grafted via vinyl groups onto porous Hap using AIBN as an initiator; 60 mmol of MMA and 1.0 mol % of AIBN were dissolved in 10 ml of anhydrous DMF. Six MOI-modified porous Hap blocks were immersed in the MMA monomer solution in a 40 ml glass bottle. Graft polymerization was achieved in a nitrogen atmosphere at 60 °C for 24 h. PMMA-grafted porous Hap was copiously washed three times with DMF followed by ethanol washing twice to remove ungrafted homopolymer, and the block was then dried under reduced pressure for 24 h.

3. Results and discussion

3.1. Porous hydroxyapatite

XRD profiles of porous Hap cement unsintered and sintered at 800, 1000, and 1200 °C are shown in Fig. 1(a)–(d). Initially, the reaction between MCPM and $CaCO_3$ formed brushite ($CaHPO_4 \cdot 2H_2O$, DCPD) and simultaneously produced CO_2 gas making interconnecting holes in the bulk [5]. After DCPD and TCPM

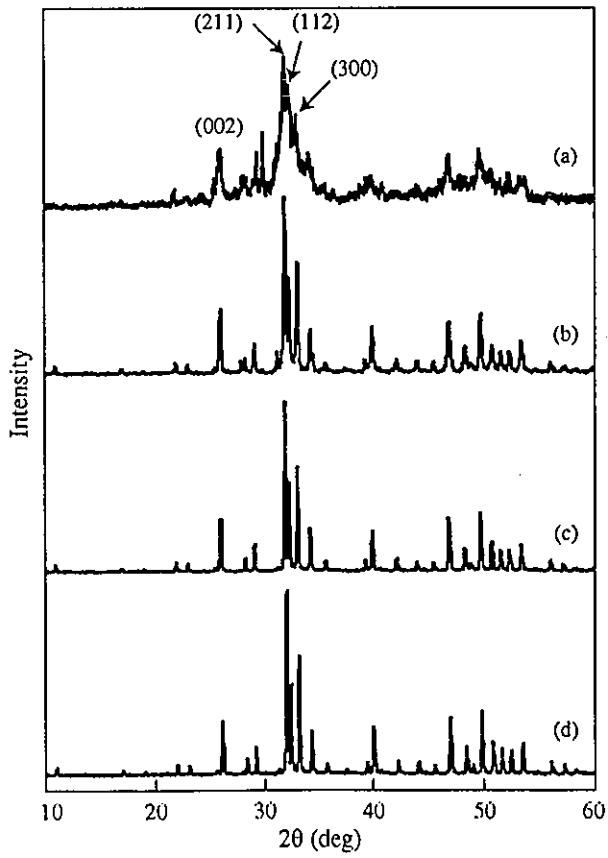

Figure 1 XRD profiles of porous Hap; (a) unsintered; sintered at (b) 800 °C, (c) 1000 °C, and (d) 1200 °C.

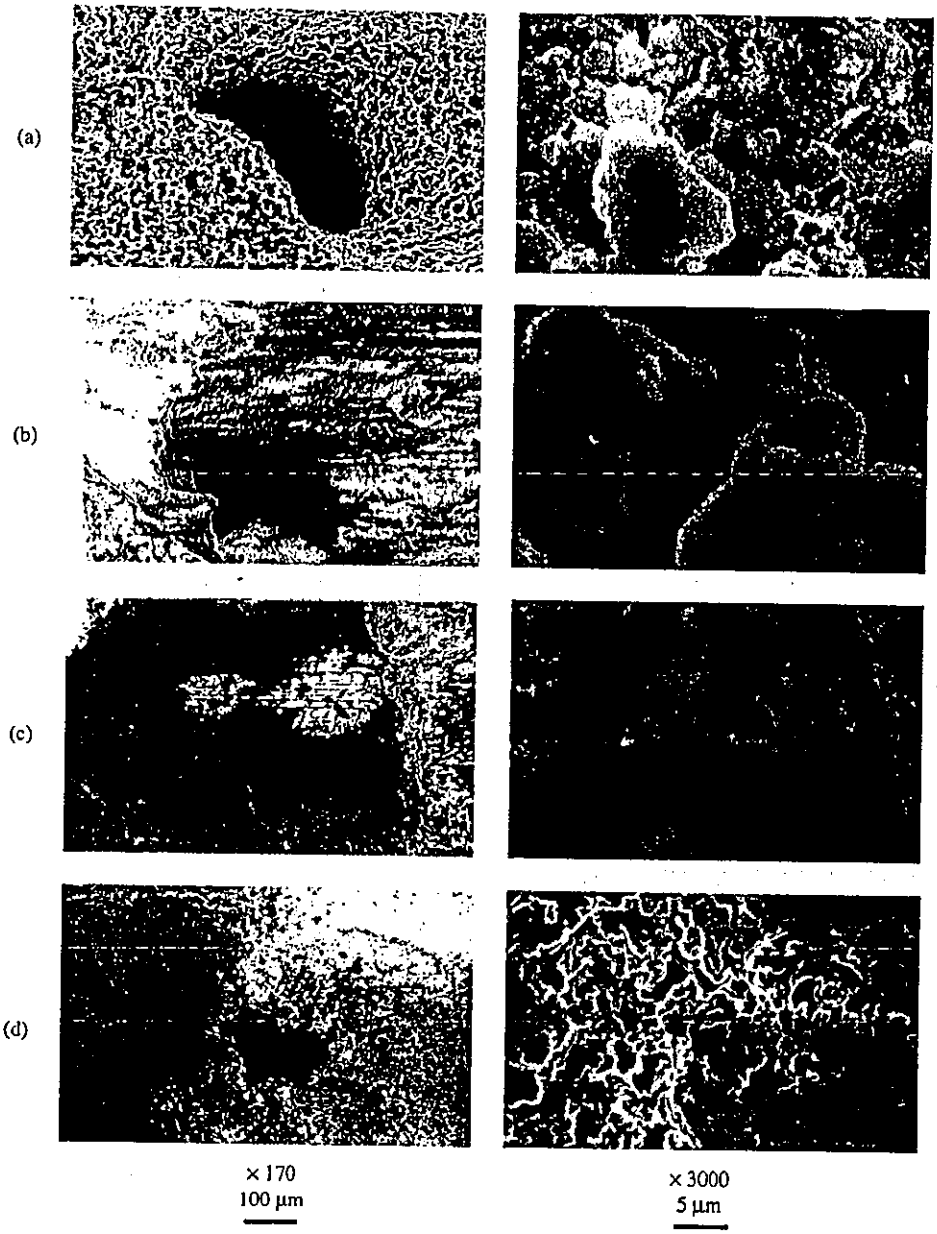

Figure 2 SEM micrographs of porous Hap; (a) unsintered; sintered at (b) 800 °C, (c) 1000 °C, and (d) 1200 °C.

were reacted in the NaOH solution for 3 days, the cement converted to Hap (Fig. 1(a)). With increasing sintering temperature, Hap peaks at (0 0 2), (2 1 1), (1 1 2), and (3 0 0) become sharper due to increasing crystallinity.

Fig. 2 shows a SEM micrograph of samples of macropores and microstructures. The macropore size decreased from 200 to 100 nm with increasing sintering temperature. Hap crystal growth by sintering changed pore size and crystal shape. The microstructure of porous Hap sintered at 800 °C showed a microrugged structure. Samples sintered at 1000 and 1200 °C, however, had a smooth structure. Yubao *et al.* [22] reported that calcium-deficient apatite particles melt about these temperatures, so this change in porous Hap crystal microstructure may be caused by Hap crystal melting during heating from 800 to 1000 °C.

3.2. Introduction of vinyl groups

Porous Hap was chemically modified with MOI monomer in an anhydrous system. Di-*n*-butyltin (IV) dilaurate as a catalyst effectively promoted the reaction between the isocyanate group and hydroxyl groups [23]. We plotted the amount of MOI monomer on porous Hap against reaction time at 60 °C (solid symbols, Fig. 3) determined using TG-DTA to calculate weight loss between room temperature and 600 °C. Open symbols show the amount of MOI monomer on porous Hap calculated by titration to determine the amount of vinyl groups contributing to polymerization [24–26].

It was clear that the polymerization-reaction of MOI by heating during the modification-reaction of the MOI monomer on/in the porous Hap did not occur because the amounts to MOI calculated through the TG-DTA and the titration for 24 h of reaction time took almost same value. MOI monomer added for a 24 h reaction with porous Hap sintered was calculated as 0.11 mmol/g at 800 °C, 0.044 mmol/g at 1000 °C, and 0.038 mmol/g at 1200 °C. In nonsintered Hap powder (BET-specific surface area of 66 m^2/g), Liu *et al.* reported that the amount modified with MOI monomer increased with increasing reaction time, finally reaching equilibrium of about 0.7 mmol/g in both reaction conditions at 50 °C/20 h and 70 °C/12 h [20]. The difference in reaction kinetics between porous

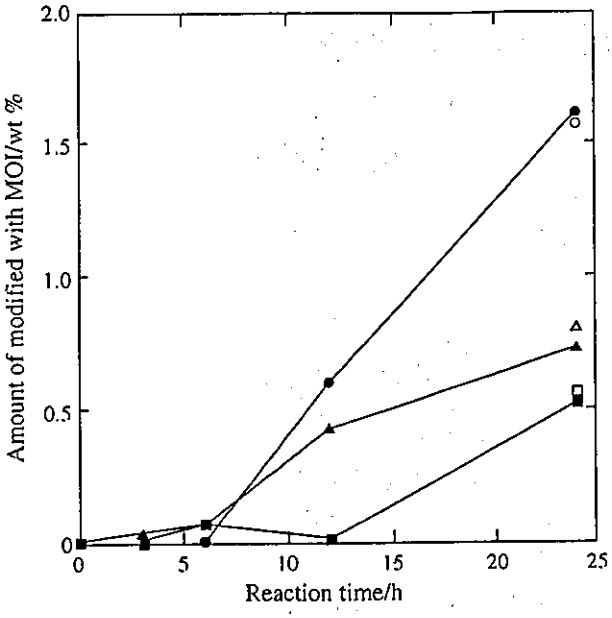

Figure 3 Weight gain of MOI monomer on porous Hap as a function of reaction time; sintered at (●) 800 °C, (▲) 1000 °C, and (■) 1200 °C. Open symbols were determined by titration.

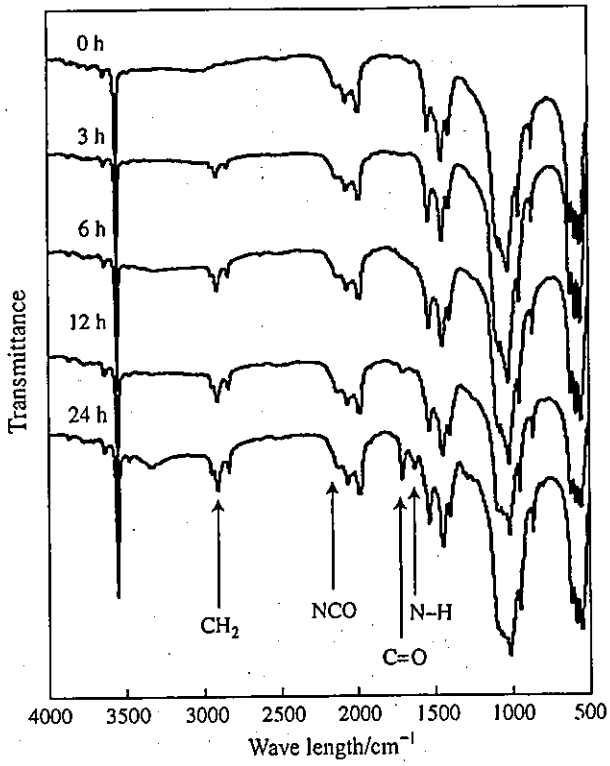

Figure 4 FT-IR spectra of MOI-modified porous Hap sintered at 800 °C. FT-IR spectra of MOI-modified porous Hap sintered at 1000 and 1200 °C were almost identical.

Hap and Hap powder is considered due to the restriction of MOI monomer diffusion to the inside of porous Hap and because the surface area of porous Hap able to react with MOI monomer was much less compared to Hap powder.

In FT-IR spectra of MOI-modified porous Hap sintered at 800 °C (Fig. 4), absorption at 2960 cm^{-1} is attributable to the stretching vibration of C–H, which increased with increasing MOI monomer on porous Hap. The presence of the deformation vibration of the amide N–H peak at 1660 cm^{-1} and of the stretching vibration of the ester C=O peak at 1730 cm^{-1} indicated that MOI monomer and porous Hap were coupled by covalent linkage, the peak attributed to the isocyanate group (–NCO) was clear at 2270 cm^{-1} in the spectrum of the MOI monomer [27]. The isocyanate group peak completely disappeared after MOI monomer was added to porous Hap (Fig. 4), indicating the isocyanate group of the MOI monomer reacted completely with Hap hydroxyl groups under our reaction conditions. The peak of about 1450 cm^{-1} corresponded to ν_3CO_2, the broad band over 1000–1150 cm^{-1} corresponded to ν_3PO_4, the peak of about 630 cm^{-1} corresponded to δOH, and the peaks of about 570 and 600 cm^{-1} to the ν_4PO_4, indicating Hap formation.

Fig. 5 shows SEM observations of MOI-modified porous Hap at low and high magnification. Macro- and microchannels of porous Hap were unchanged by MOI monomer modification compared to Fig. 1, implying that MOI monomer was coated as a thin layer on porous Hap.

3.3. Graft polymerization with MMA

MMA was graft-polymerized on porous Hap through vinyl groups in the MOI monomer using AIBN as a polymerization initiator. We determined the amount of PMMA grafting on MOI-modified porous Hap using TG-DTA (Table I). When graft polymerization with MMA was done using un-modified porous Hap, the amount of graft polymerization of PMMA was zero after washing with DMF. Table I shows that weight gain refers only to the amount of grafting PMMA on porous Hap attached by covalent bonding. MMA grafted on porous Hap sintered at 800 °C was significantly lower compared to that sintered at 1000 and 1200 °C, although MOI modification on porous Hap sintered was significantly higher. There might be two reasons to explain this phenomenon: first, MMA monomer is difficult to diffuse and react the vinyl groups in the micro-cavity of the 800 °C sintered porous Hap, since it has the micro-rugged structure as shown in Fig. 5. Second, sintered porous Hap at 800 °C has too small space that limits the growth reaction of the PMMA graft chain.

FT-IR spectra of PMMA homopolymer and PMMA-grafted porous Hap are shown in Fig. 6. Compared with

TABLE I Weight% of add-on MOI, grafting PMMA, and compressive strength of porous Hap

Sintered temperature/°C	MOI add-on/ wt%	Grafting polymer (PMMA)/wt%	Compressive strength at intact porous Hap/MPa	Compressive strength at PMMA grafted porous Hap/MPa
800	1.62	2.84	1.54	10.3
1000	0.68	6.97	3.24	21.2
1200	0.59	6.27	17.3	47.1

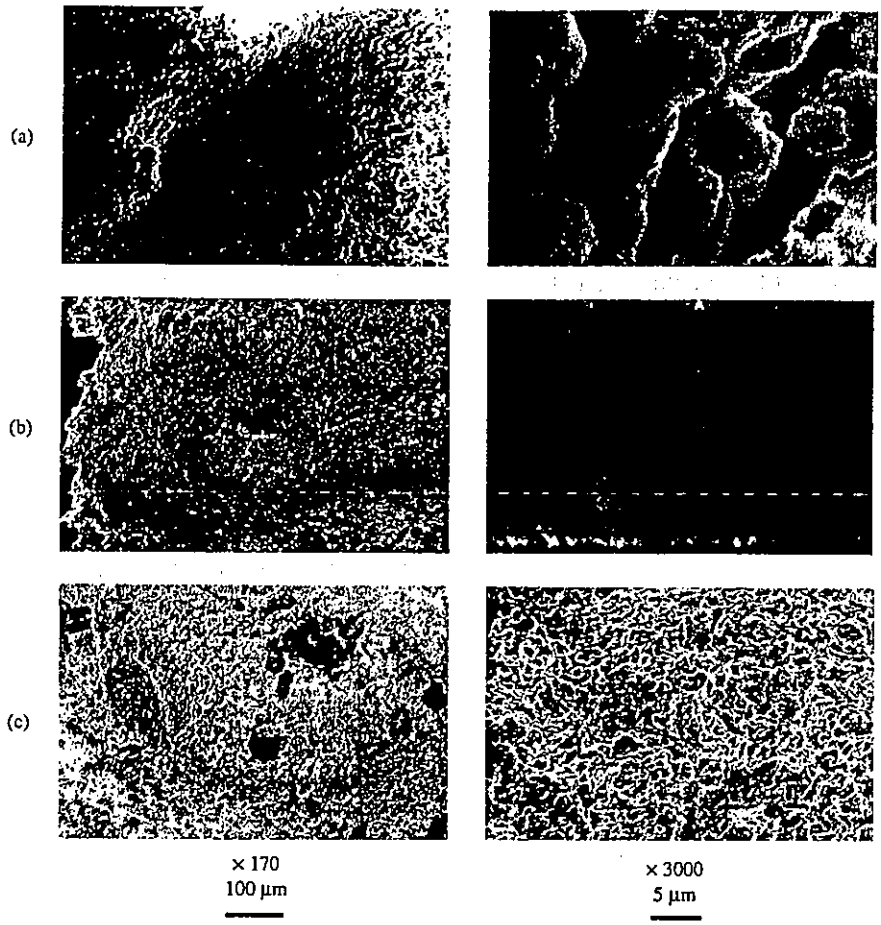

Figure 5 SEM micrographs of MOI-modified porous Hap; sintered at (a) 800 °C, (b) 1000 °C, and (c) 1200 °C.

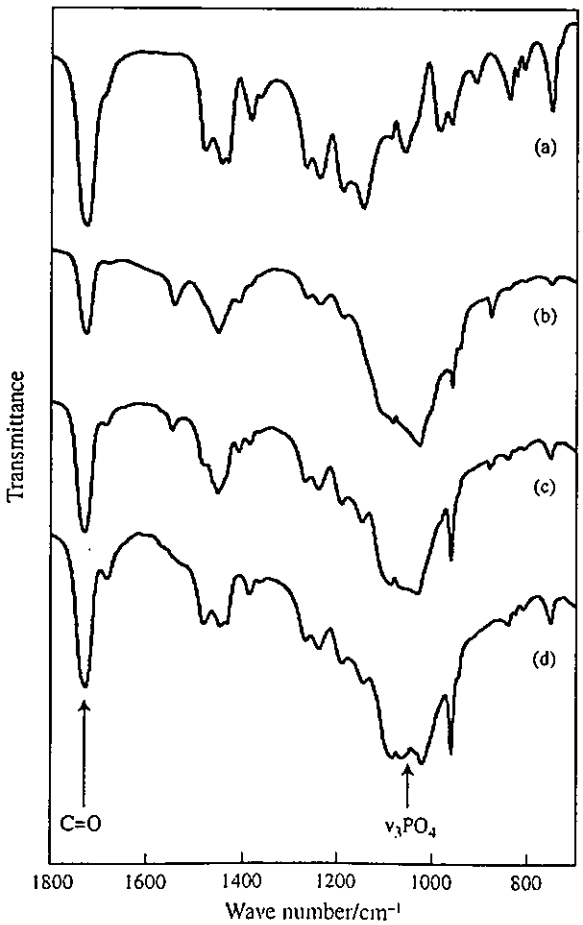

Figure 6 FT-IR spectra of PMMA-grafted porous Hap; (a) PMMA homopolymer; sintered at (b) 800 °C, (c) 1000 °C, and (d) 1200 °C.

Fig. 4, absorption at about 1730 cm^{-1} attributed to the ester C=O peak increased with increasing PMMA grafting, clearly showing that PMMA was grafted successfully on porous Hap. The ratio of the peak strength between the C=O and the PO_4 band of porous Hap sintered at 800 °C (Fig. 6(b)) indicates that the amount of grafted PMMA was less than that of samples sintered at 1000 (c) and 1200 °C (d), which agreed well with PMMA grafted on Hap (Table I).

The compressive strength of intact porous Hap sintered at 800, 1000, and 1200 °C (Table I) increased with increasing sintering temperature, because the crystal growth of porous Hap and apparent density of porous Hap by melting with increasing the sintering temperature. The compressive strength of porous Hap grafted with PMMA increased 4.5 times over the sintering temperature range compared to 11.2 times for uncoated porous Hap. Porous Hap strength thus increased dramatically with this surface modification. For porous Hap sintered at 800 °C, compressive strength increased 6.7 times that of uncoated Hap, even though the amount of PMMA was low. The compressive strength of PMMA-grafted porous Hap sintered at 1000 °C was roughly half that sintered at 1200 °C, although the amount of PMMA grafted on porous Hap sintered at 1000 and 1200 °C was similar. These results indicate that compressive strength could be greatly affected by grafting a thin layer of PMMA on Hap, so we can synthesize porous Hap having desired mechanical properties over a wide range from 1.5 to 47 MPa by controlling the sintering temperature of Hap blocks to be coated and the amount of PMMA then to be grafted.

4. Conclusions

We developed a way to modify the porous Hap surface through an introduced functional group attached by covalent linkage. PMMA provided porous Hap with mechanical and biostable properties through bonding to a vinyl group coupled on porous Hap. PMMA was used as an example polymer for interaction with the Hap surface modified by MOI. This two-step surface modification of Hap is widely applicable to graft polymerization with a vinyl polymer and conjugation with biomolecules, such as proteins or oligopeptides [28], to improve Hap mechanical properties and functionality. We are now developing a 3-dimensional cell-culture vessel and biomolecule separator using porous Hap cartridges grafted with vinyl- and biopolymers.

References

1. I. SOTEN and G. A. OZIN, *J. Mater. Chem.* 9(3) (1999) 703.
2. L. C. CHOW, *J. Ceram. Soc. Japan.* 99(10) (1991) 954.
3. M. KIKUCHI, S. ITOH, S. ICHINOSE, K. SHINOMIYA and J. TANAKA, *Biomaterials* 22 (2001) 1705.
4. D. WALSH and S. MANN, in "Handbook of Biomimetics", vol. S6, edited by Y. Osada (NTS Inc., Tokyo, Japan, 2000) 59, Chapter 1.
5. D. WALSH, T. FURUZONO and J. TANAKA, *Biomaterials* 22 (2001) 1205.
6. P. YLINEN, M. RAEKALLIO, T. TOIVONEN, K. VIHTONEN and S. VAINONPAA, *J. Oral Maxillofac. Surg.* 49 (1991) 1191.
7. R. W. BUCHOLZ, A. CARLTO and R. HOLMES, *Clin. Orthop.* 240 (1989) 53.
8. T. M. CHU, D. G. ORTON, S. J. HOLLISTER, S. E. FEINBERG and J. W. HALLORAN, *Biomaterials* 23(5) (2002) 1283.
9. S. JOSCHEK, B. NIES, R. KROTZ and A. GOFERICH, *ibid.* 21(16) (2000) 1645.
10. W. J. BIGHAM, P. STANLEY, J. M. CAHILL JR, R. W. CURRAN and A. C. PERRY, *Ophthal. Plast. Reconstr. Surg.* 15(5) (1999) 317.
11. B. K. VAUGHN, A. V. LOMBARDI JR and T. H. MALLORY, *Semin. Arthoplasty.* 2(4) (1991) 309.
12. G. JIANG and D. SHI, *J. Biomed. Mater. Res.* 43(1) (1998) 77.
13. A. M. P. DUPRAZ, J. R. DE WIJN, S. A. T. VAN DER MEER and K. DE GROOT, *ibid.* 30 (1996) 231.
14. K. NISHIZAWA, M. TORIYAMA, T. SUZUKI, Y. KAWAMOTO, Y. YOKUGAWA and F. NAGATA, *Chem. Soc. Jpn.* 1 (1995) 63.
15. J. C. BEHIRI, M. BRADEN, S. KHORASANI, D. WIWATTANADATE and W. BONFIELD, in "Bioceramics", vol. 4, edited by W. Bonfield, G. W. Hastings and K. E. Tanner (Elsevier Science, London, 1991) 301.
16. D. N. MISRA, *J. Dent. Res.* 12 (1985) 1405.
17. Q. LIU, J. R. DE WIJN, M. VAN TOLEDO, D. BAKKER and C. A. VAN BLITTERSWIJK, *J. Mater. Sci.: Mater. Med.* 7 (1996) 551.
18. V. DELPECH and A. LEBUGLE, *Clin. Mater.* 5 (1990) 209.
19. J. DANDURAND, V. DELPECH, A. LEBUGLE, A. LAMURE and C. LACABANNE, *J. Biomed. Mater. Res.* 24 (1990) 1377.
20. Q. LIU, J. R. DE WIJN and C. A. VAN BLITTERSWIJK, *ibid.* 40(3) (1998) 490.
21. R. LABELLA, M. BRADEN and S. DEB, *Biomaterials* 15 (1994) 1197.
22. L. YUBAO, C. P. A. T. KLEIN, J. DE WIJN and S. VAN DE MEER, *J. Mater. Sci.: Mater. Med.* 5 (1994) 263.
23. M. R. THOMAS, *J. Coat. Technol.* 55 (1983) 55.
24. A. BAYER, *Ann.* 245 (1888) 103.
25. H. MEYER, *Ber.* 28 (1895) 2965.
26. R. MEYER and E. HARTMANN, *ibid.* 38 (1905) 3956.
27. T. FURUZONO, K. ISHIHARA, N. NAKABAYASHI and Y. TAMADA, *Biomaterials.* 21 (2000) 327.
28. G. T. HERMANSON, "Bioconjugate Techniques" (Academic Press, Inc., New York, 1996).

Received 15 August 2002
and accepted 3 June 2003

Novel Guglielmi Detachable Coils (GDCs) for the Treatment of Brain Aneurysms. *In Vitro* study of Hydroxyapatite Coating on Pt Plate as GDCs Model

Michiya Matsusaki,[1] Takashi Kamezawa,[2] Tetsuro Shimozuru,[2] Jun-ichi Kuratsu,[2] Akio Kishida,[3] Mitsuru Akashi[1]

[1] Department of Nanostructured and Advanced Materials, Graduate School of Science and Engineering, Kagoshima University, 1-21-40 Korimoto, Kagoshima 890-0065, Japan

[2] Department of Neurosurgery, Faculty of Medicine, Kagoshima University, 8-35-1 Sakuragaoka, Kagoshima 890-8520, Japan

[3] Department of Biomedical Engineering, National Cardiovascular Center Research Institute, 5-7-1 Fujishiro-dai, Suita, Osaka 565-8565, Japan

Received 12 July 2002; revised 20 December 2002; accepted 26 December 2002
Published online 5 June 2003 in Wiley InterScience (www.interscience.wiley.com). DOI: 10.1002/jbm.b.10030

Abstract: **With the use of an alternate soaking process a thin layer of hydroxyapatite (HAp) was formed on a platinum plate (Pt plate) which was used as a model for Guglielmi detachable coils (GDCs). The *in vitro* coagulant activity of the HAp-coated Pt plate was evaluated for the purpose of brain aneurysm treatment. In order to fix and to form the apatite layer homogeneously, β-mercaptopropionic acid was immobilized onto the Pt surface prior to use. The HAp layer was formed on the β-mercaptopropionic acid-fixed Pt plate surface, and quantitative control of apatite formation was achieved by controlling the number of alternate soaking process cycles. The HAp formed on the Pt plate surface was confirmed by X-ray diffraction and X-ray photoelectron spectroscopy studies. Blood interaction with the Pt plate was altered from nonthrombotic to highly thrombotic by forming a HAp layer on the surface. The alternate soaking process is an appropriate method to modify the GDCs. Complete treatment of brain aneurysms is expected with the use of HAp-coated GDCs, which would allow formation of a stable blood clot.** © 2003 Wiley Periodicals, Inc. J Biomed Mater Res Part B: Appl Biomater 66B: 429–438, 2003

Keywords: **Guglielmi detachable coils (GDCs); platinum plate (Pt plate); aneurysms; hydroxyapatite (HAp); alternate soaking process; thrombus formation**

INTRODUCTION

Guglielmi detachable coils (GDCs) embolization for the treatment of brain aneurysms was first introduced by Guglielmi in 1991[1,2] and has become an integral part of the treatment strategy for cerebral aneurysms throughout the world.[3,4] Recent clinical reports indicate that complete occlusion can be achieved in more than 80% of small-sized/small-necked aneurysms by the GDC technique. However, the GDC technique is less effective for the treatment of wide-necked aneurysms (size > 4 mm), because coil herniation out of the aneurysm forces the operator to loosely pack the aneurysm.[5] Loose GDC packing in an aneurysm promotes a high incidence of aneurysm recanalization and coil compaction. Another weak point of the GDC technique is that it can produce only a limited cellular response in the aneurysm clot. This is considered to be the major cause of the delay in the development of neoendothelial coverage across the neck of the aneurysm, which allows for coil compaction with concomitant aneurysm recanalization and regrowth. The reason for these weaknesses is the biological inertness of the GDCs. The GDCs are made of platinum, which is biologically inert. Therefore, if the surface of the GDC is made more biologically active, aneurysm formation and neoendothelial coverage across the neck of the aneurysms will accelerate.

Several modifications to the surfaces of the GDCs have been reported, including the immobilization of extracellular matrix (ECM) proteins and coating with cytokines such as growth factors.[6–8] Murayama et al. studied coating Type I collagen, fibronectin, vitronectin, laminin, and fibrinogen onto GDCs.[9] They reported that when the coated GDCs were

Correspondence to: Mitsuru Akashi, Department of Nanostructured and Advanced Materials, Graduate School of Science and Engineering, Kagoshima University, 1-21-40 Korimoto, Kagoshima 890-0065, Japan (e-mail: akashi@apc.kagoshima-u.ac.jp)

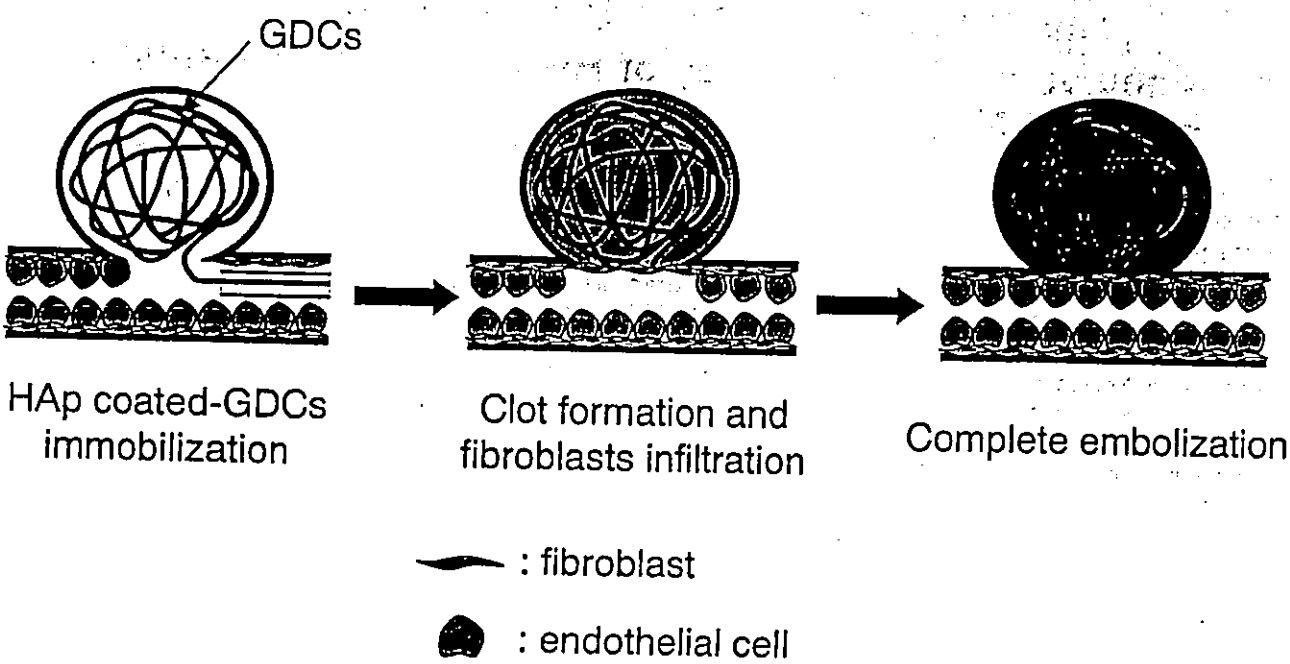

Figure 1. Brain aneurysm treatment strategy used here.

used, a well-organized fibrous tissue bridging across the aneurysm's neck was observed. Their studies indicated that coating with bioactive substances was effective.

On the basis of the results of past research, the complete mbolization mechanism of aneurysms by GDCs is believed o be as follows. First, a thrombus is formed around the GDCs nside the aneurysm, fibroblasts infiltrate the thrombus, and ndothelial cells are induced on the thrombus surface. After eointimal formation, an anticoagulant surface is formed. Consequently, it is expected that the induction and proliferation of endothelial cells are essential for perfect occlusion and healing.

The strategy in this article was to coat a coagulant substance onto the surfaces of the GDCs. It is expected that a thrombus will be rapidly formed, inducing the proliferation of endothelial cells. Hydroxyapatite [HAp: $Ca_{10}(PO_4)_6(OH)_2$] was used as the coating material. HAp, which is one of the main components of bone, is a biofunctional inorganic ma-

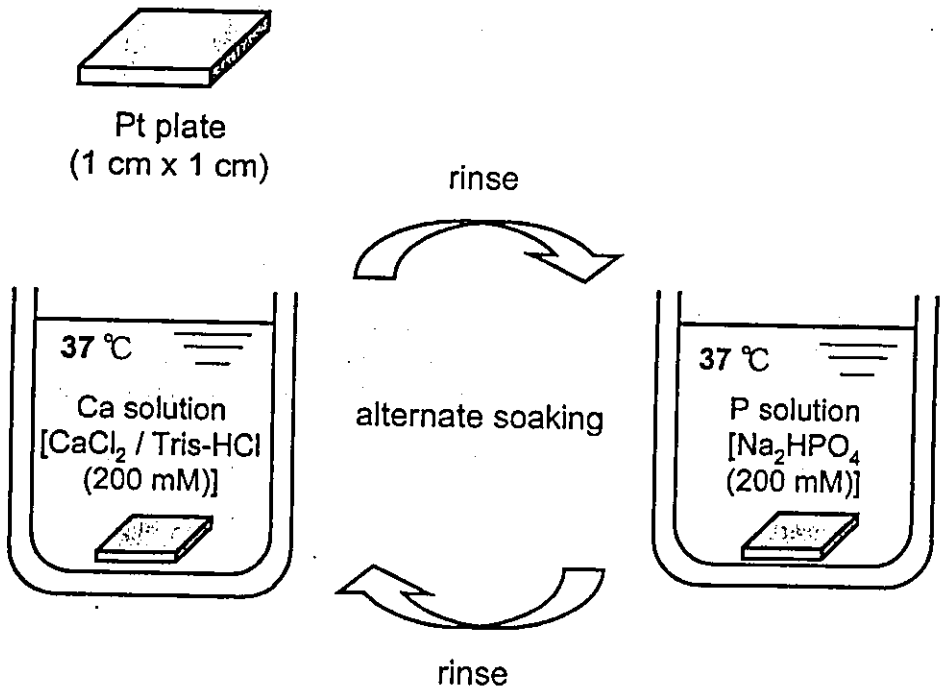

Figure 2. The alternate soaking process used in this study.

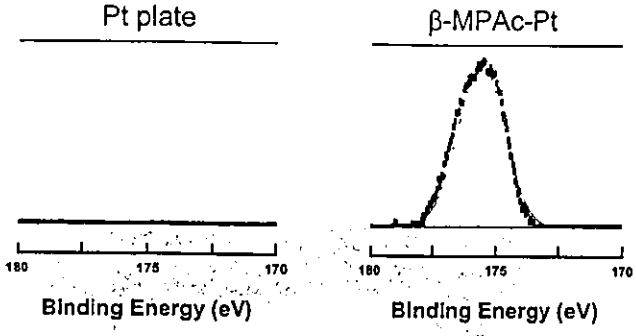

Figure 3. High-resolution XPS spectra of the S_{2p} peak for the Pt plate and β-MPAc-Pt.

terial. In many orthopedic and tissue adhesive applications, researchers have reported the use of polymer- or metal-HAp composites.[10–12] Coating a HAp layer onto a substrate can be accomplished by many techniques, such as plasma spraying,[13] a biomimetic process,[14] and conventional frame spraying.[15] It has been reported that bone-like HAp could be formed in the desired amount on/in a three-dimensional structured matrix at normal temperatures and pressure with the use of a novel alternate soaking process. This soaking process was successfully used for coating HAp on various kinds of surfaces, such as hydrogel, resin, and metal.[16–19]. It is expected that the brain aneurysm treatment will be accelerated by HAp coating on the surfaces of GDCs (Figure 1). HAp coating and thrombus formation on the platinum surface were evaluated with the use of a platinum plate as a model of the GDCs in the present study. Early and tight thrombus formation in the aneurysm is expected to lead to early neointima formation. Thus, HAp coating on GDCs should lead to a drastic improvement in aneurysm treatment.

MATERIALS AND METHODS

Materials

β-mercaptopropionic acid was purchased from Tokyo Kasei (Tokyo, Japan). All other chemicals were purchased from Wako Pure Chemical Industries (Osaka, Japan), Aldrich (Milwaukee, WI), and Santoku Chemical Industries (Tokyo). Platinum coated plastic plates (Pt plate) were purchased from Tanaka Precious Metal Industries (Tokyo).

Self-Assembled Monolayer (SAM) Formation on Pt Plate

The SAM formation method used here was based on Aizenberg's method with minor modifications.[22] Before apatite coating, the Pt plate was treated two times with a piranha solution (H_2SO_4:H_2O_2 = 3:1) for 1 min each time, followed by rinsing with pure water and drying with N_2 gas in order to clean its surface. The cleaned Pt plate was then immersed in a 10-mM solution of β-mercaptopropionic acid in ethanol for 1 h. The immobilization of β-mercaptopropionic acid onto the Pt plate was confirmed by X-ray photoelectron spectroscopy (XPS). Afterward, the apatite was deposited onto the Pt plate surface.

Apatite Coating of Pt Plate

Apatite coating onto the β-mercaptopropionic acid immobilized on the Pt plate was performed as shown in Figure 2.

Step 1: The Pt plate (1 cm × 1 cm) was soaked in 300 ml of $CaCl_2$ (200 mM) (Ca solution) at 37 °C for a predetermined period of time.

Step 2: The Pt plate was removed from the Ca solution, and rinsed with excess distilled water at 37 °C 10 times.

Step 3: The Pt plate was subsequently soaked in a Na_2HPO_4 (120 mM) (P solution) at 37 °C for a predetermined period of time.

Step 4: Similar to the Ca solution, the Pt plate was removed from the P solution and rinsed with excess water at 37 °C 10 times.

With the use of these four steps, the apatite coating on the Pt plate was deposited by alternately soaking the plate in the Ca and P solutions.

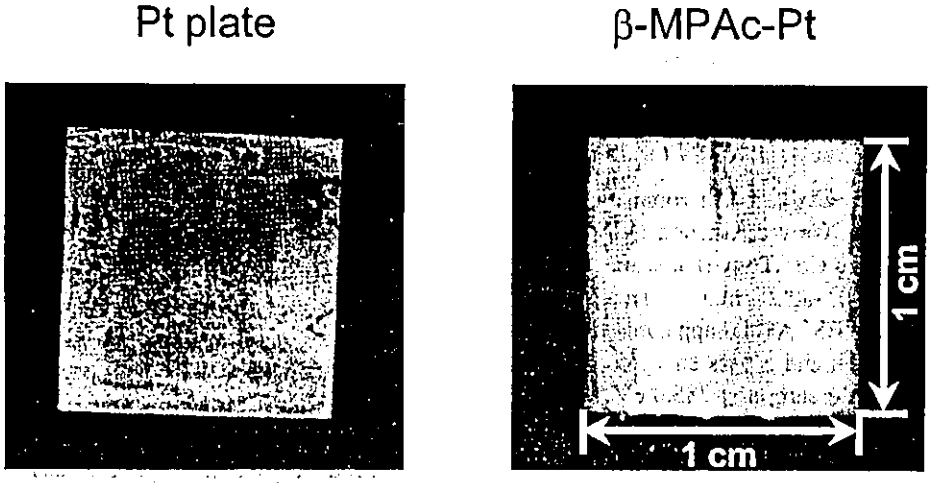

Figure 4. Macroscopic observation of the Pt plate and β-MPAc-Pt after 50 alternate soaking cycles.

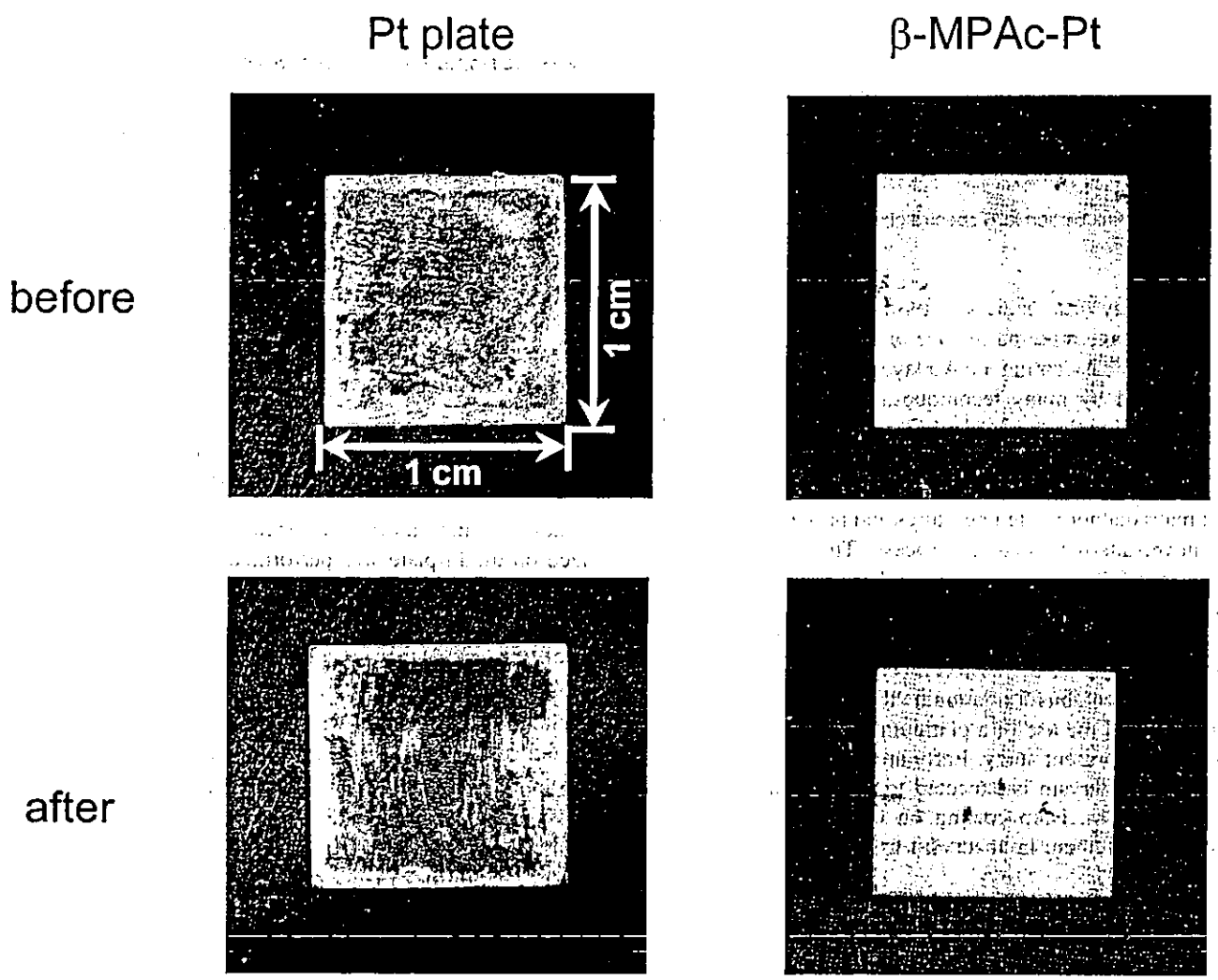

Figure 5. Results of the peeling test.

The Peeling Test

Scotch tape (1.5 × 2.0 cm) was placed on the samples, and a 50-g weight was put on the scotch tape. Ten seconds later, the weight and scotch tape were removed, and the sample surface was observed.

Analysis of the Apatite-Coated Pt Plate

he apatite-coated Pt plate was dried at room temperature vernight, and analyzed by X-ray diffraction (XRD) with a eigerflex RAD-IIB (Rigaku Co., Tokyo) at scanning angles hat ranged from 50 to 10° at 2° min^{-1}. The XPS was erformed with a Shimadzu ESCA1000 apparatus employing gKα radiation (1253.6 eV) and a pass energy of 31.5 eV. he peaks were referenced to carbon at 285.0 eV to account or sample charging. The Pt plate and the apatite-coated Pt late surfaces were observed by scanning electron microsopy (SEM) with a HITACHI S-4100H SE microscope.

Thrombus Formation Test

ne milliliter of human whole blood, which was collected ith a 21-gauge needle from healthy adult volunteers, was injected into tubes containing the samples. These tubes were allowed to stand at 37 °C. After a fixed time, the samples were taken out and washed with phosphate-buffered saline.

RESULTS AND DISCUSSION

Immobilization of β-Mercaptopropionic Acid onto a Pt Plate

When a virgin platinum surface was used, a nonhomogeneous HAp layer was formed by the alternate soaking process. Consequently, modification of the platinum surface was studied in order to obtain a homogeneous HAp coating layer. Tanahashi et al. reported that a homogeneous HAp layer was formed onto polar groups such as carboxyl groups, which were introduced onto hydrophobic substances by electrostatic interaction.[20] Therefore, if a carboxylic group can be immobilized on the Pt plate surface, a homogeneous HAp layer would be formed on the Pt plate surface. The self-assembled monolayer (SAM) was used in order to form a carboxylic group on the Pt plate. There are many reports on the forma-

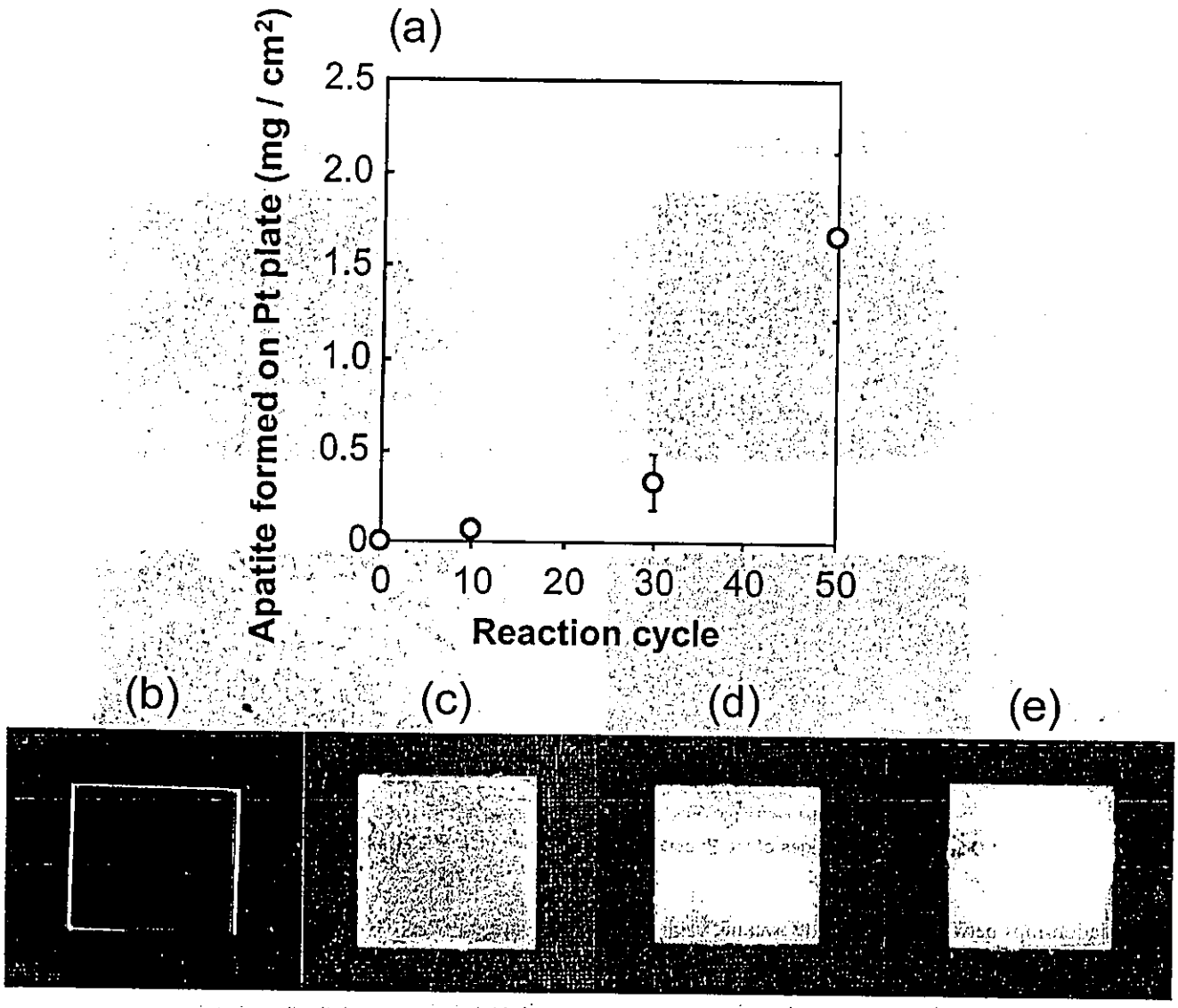

Figure 6. Relationships between the alternate soaking cycle and the amount of apatite (a), and the macroscopic observation of β-MPAc-Pt after each alternate soaking cycle [(b) 0 cycles, (c) 10 cycles, (d) 30 cycles, and (e)5 0 cycles].

tion of SAM on a gold surface; however, few studies are available on the formation of SAM on a platinum surface.[21] The immobilization of a carboxylic group on the Pt plate surface was evaluated based on the literature.[21]

The immobilization of β-mercaptopropionic acid onto the Pt plate surface was estimated by XPS. Figure 3 shows the XPS spectra of a Pt plate and β-mercaptopropionic acid immobilized onto a Pt plate (β-MPAc-Pt). The S_{2p} peak, which was attributed to the mercapto group in β-mercaptopropionic acid, was detected for β-MPAc-Pt but not for the virgin Pt plate. This result indicated that the β-mercaptopropionic acid was immobilized onto the Pt plate.

Apatite Formation on the Pt Plate

Figure 4 shows the macroscopic appearance of the Pt plate and β-MPAc-Pt after 50 alternate soaking cycles. It was clear that a homogeneous apatite layer formed on β-MPAc-Pt, but not on the Pt plate. If the apatite layer formed on the surface the GDCs could be peeled off easily, the detached apatite or clot could block the capillary vessels. Therefore, the stability on the surface as well as the homogeneity of the HAp layer is important. Figure 5 indicates the result of the peeling test. The apatite layer formed on the Pt plate was completely peeled off, whereas the apatite layer formed on β-MPAc-Pt was not peeled off. This result suggests the effect of the electrostatic interaction between the calcium in the apatite layer with the carboxyl group of β-mercaptopropionic acid. As shown in Figure 4 or 5, the immobilization of β-mercaptopropionic acid was effective in forming a homogeneous and stable apatite layer. As the process of β-mercaptopropionic acid immobilization is carried out by immersing the material into the reaction solution, it is easily applicable to the modification of the GDCs.

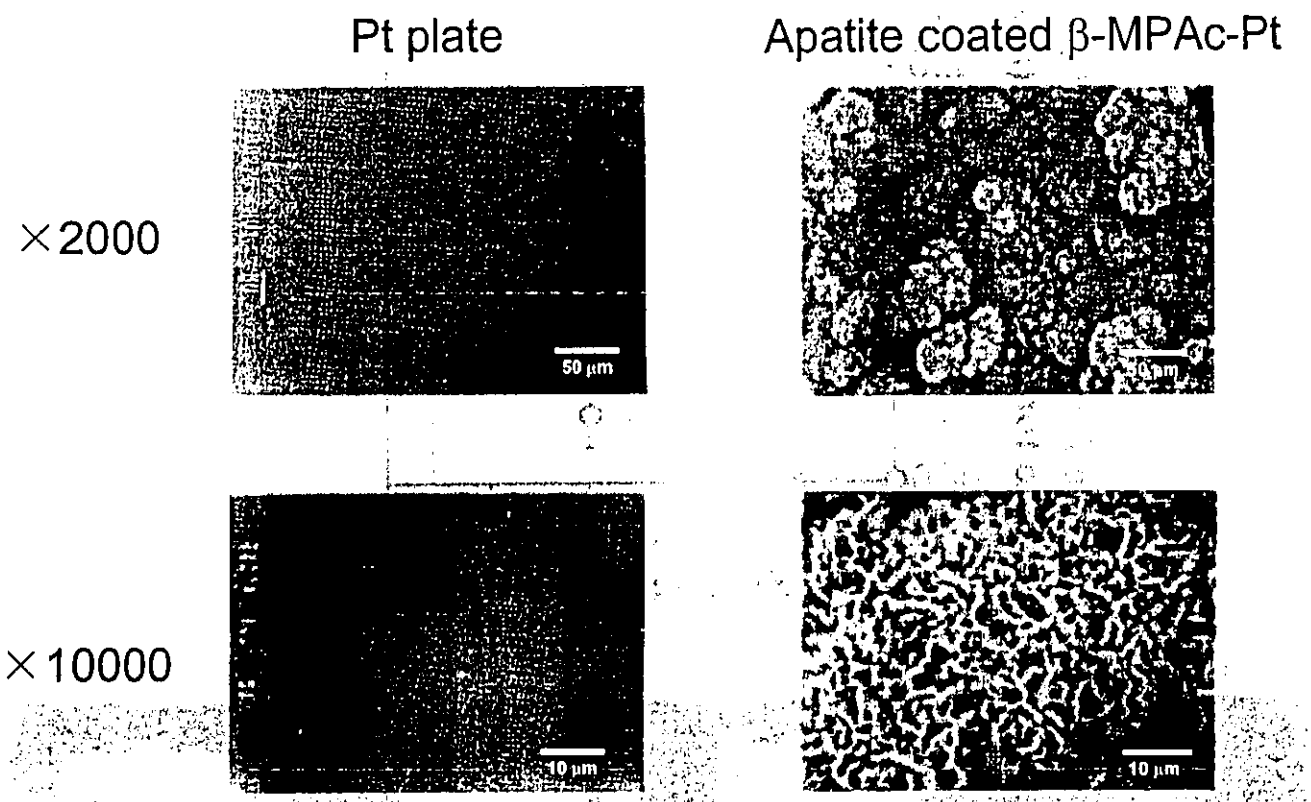

Figure 7. SEM images of the Pt plate and β—MPAc-Pt after 50 alternate soaking cycles.

The relationships between the alternate soaking cycle and the amount of HAp (a), and the macroscopic observation of β-MPAc-Pt after each alternate soaking cycle [(b) 0 cycles, (c) 10 cycles, (d) 30 cycles, and (e) 50 cycles (e)] were investigated (Figure 6). It was confirmed that the amount of HAp increased with an increasing number of alternate soaking cycles. In order to control the amount of HAp, the number of alternate soaking cycles was altered.

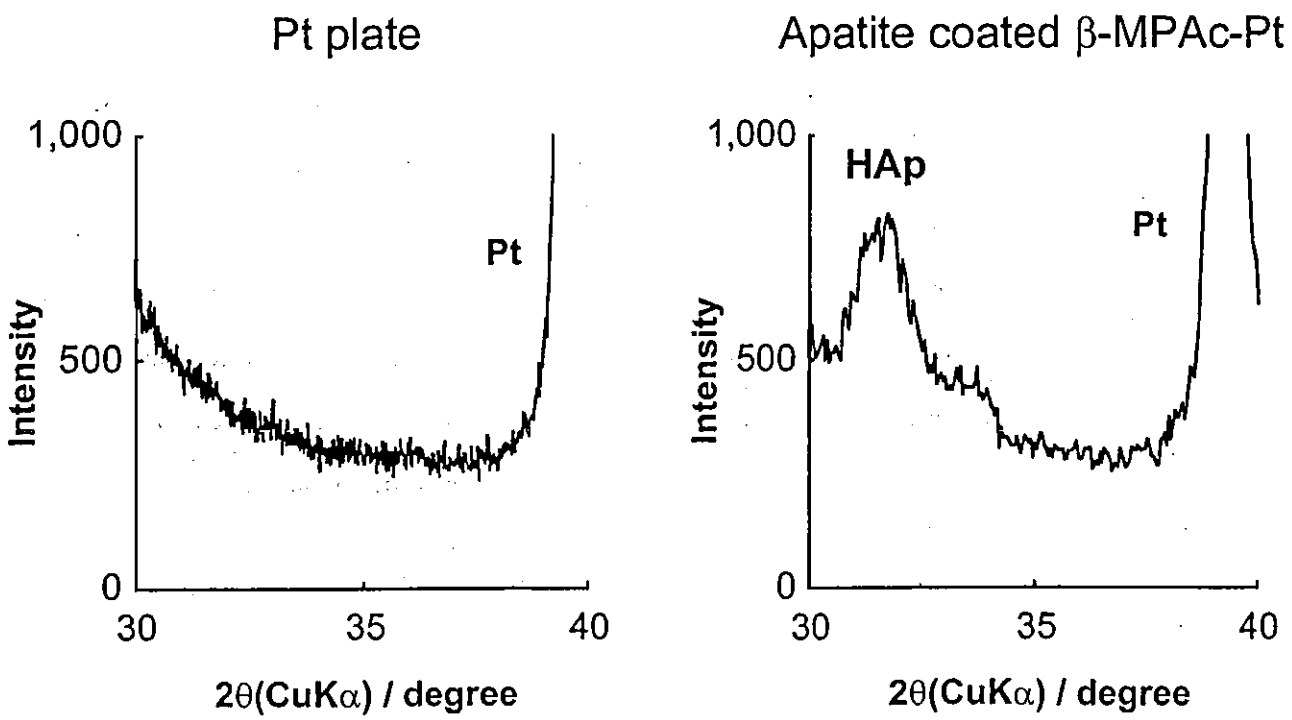

Figure 8. XRD patterns of the Pt plate and β-MPAc-Pt after 200 alternate soaking cycles.

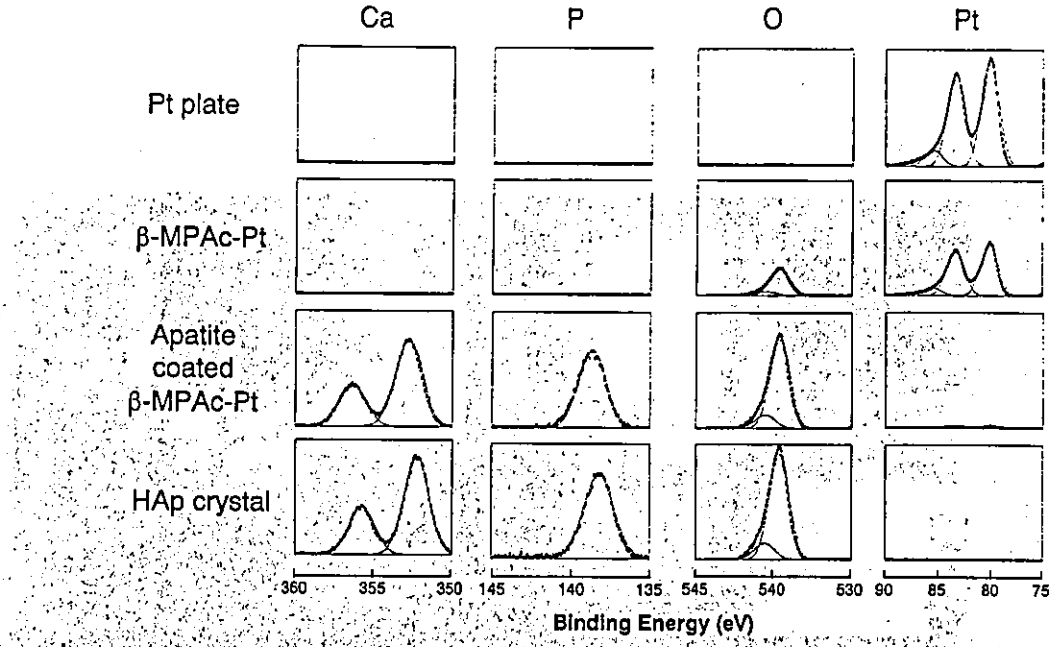

Figure 9. High-resolution XPS spectra of the Pt plate, β-MPAc-Pt, β-MPAc-Pt with HAp and commercial HAp crystal.

Analysis of the HAp-Coated Pt Plate

Figure 7 shows SEM images of the Pt plate and β-MPAc-Pt after 50 alternate soaking cycles. Aggregates of HAp crystal were observed on the Pt surface; however, the morphology of the crystals was irregular. Figure 8 shows the XRD patterns of the Pt plate and β-MPAc-Pt after 200 alternate soaking cycles. Only one platinum peak at 40° was detected in XRD patterns for the Pt plate. For β-MPAc-Pt after 200 alternate soaking cycles, a typical peak at around 32° was observed and was assigned as the main peak for the HAp crystal. Considering these results, a relatively low crystallinity for the formed HAp layer was confirmed.

Figure 9 shows the XPS spectra of the Pt plate, β-MPAc-Pt, β-MPAc-Pt with HAp (after 200 alternate soaking cycles) and commercial HAp crystal (Wako Pure Chemical Industries). With respect to β-MPAc-Pt with HAp and commercial HAp, peaks for Ca_{2p}, P_{2p}, and O_{1s} could be observed. It was confirmed that the HAp layer covered the Pt plate surface, because the peak correspond to the Pt_{4f} signal was barely detectable in the β-MPAc-Pt with HAp sample. Table I indicates the XPS peak area ratio of the Ca/P of β-MPAc-Pt with HAp and the stoichiometric ratio of HAp. The Ca/P ratio of β-MPAc-Pt with HAp was 1.40, which was somewhat different from the stoichiometric ratio (Ca/P = 1.67). Accordingly, the amount of Ca and P was quantified by the other methods. β-MPAc-Pt with HAp was dissolved in 1N-HCl for 1 day [$Ca_{10}(PO_4)_6(OH)_2 + 8H^+ \rightarrow 10Ca^{2+} + 6HPO_4^{2-} + 2H_2O$]). The amount of dissolved phosphorus ion and calcium ion was analyzed by the molybdenum blue method[22] and the orthocresolphthalein method,[23] respectively. The Ca/P ratio was 1.37, which was nearly equal to the result of XPS peak area ratio (data not shown). The difference may have been caused by the presence of defective apatite ($Ca_{10-u}(HPO_4)_u(PO_4)_{6-u}(OH)_{2-u}$; Ca/P = (10 − u)/6), octacalcium phosphate (OCP; Ca/P = 1.33) or β-tricalcium phosphate (β-TCP; Ca/P = 1.50).[24] The Ca_{2p} and P_{2p} peaks were observed after only 1 cycle of the alternate soaking process. To avoid the formation of a weakly bound layer of HAp, the number of cycles for the alternate soaking process was set to one for the experiments that followed.

TABLE I. XPS Peak Area Ratio of Ca/P of β-MPAc-Pt with HAp and Stoichiometric Ratio of HAp

	β-MPAc-Pt with HAp	Stoichiometric Ratio
Ca/P	1.40	1.67

Thrombus Formation Test

The *in vitro* coagulant activity of β-MPAc-Pt after one alternate soaking cycle was evaluated in order to examine the thrombus formation activity of the HAp layer on the β-MPAc-Pt formed. Figure 10 demonstrates thrombus formation on the Pt plate and on β-MPAc-Pt. On the Pt plate, thrombus formation was not observed after 30 min, whereas blood in the bulk phase was clotted. On the other hand, complete blood clotting was observed on β-MPAc-Pt after 10 min. This result shows that the HAp layer on β-MPAc-Pt worked as a coagulant and as a clot-adhesive substance. There was no effect on clot formation when the amount of HAp was varied (Figure 11). This indicated that the thrombus formation activity of the HAp on β-MPAc-Pt was independent of the amount of HAp formed. In the case of the GDCs,

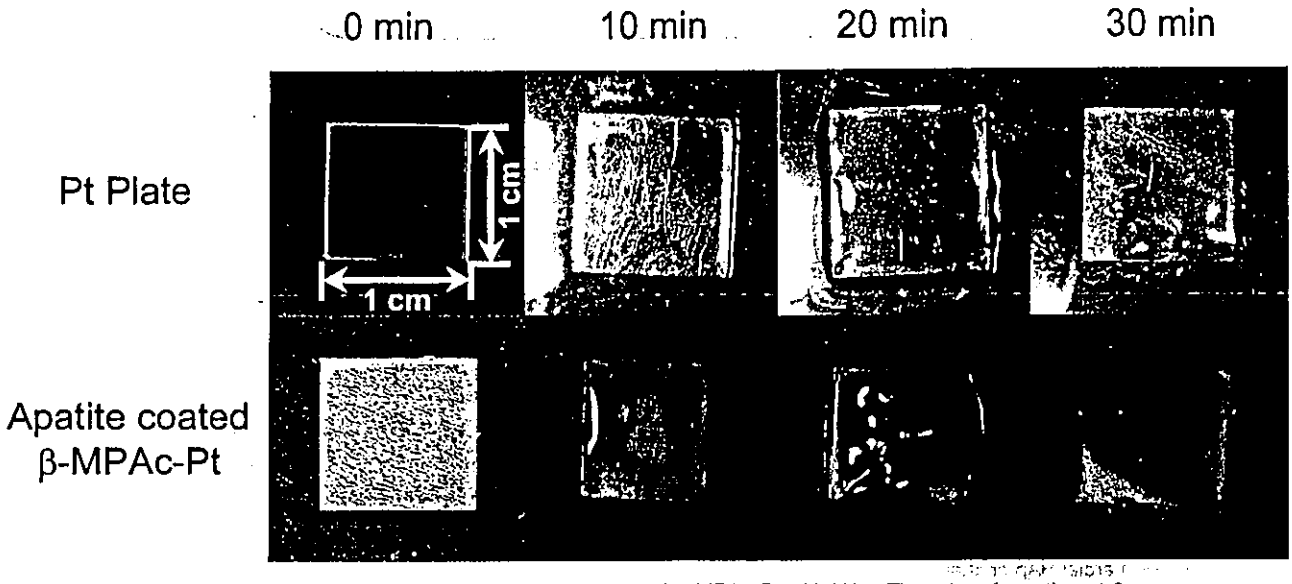

Figure 10. Thrombus formation on the Pt plate and β-MPAc-Pt with HAp. Thrombus formation at 0, 10, 20, and 30 min after immersion in blood was evaluated.

t is expected that thrombus formation and coverage of the hrombus surface by fibroblasts will be accelerated by HAp ormation on the surfaces of the GDCs.

The brain aneurysm operation is performed under heparin dministration. The thrombus formation activity of the HAp layer on β-MPAc-Pt was evaluated with human whole blood under existing heparin. Figure 12(a) shows the results of the clotting test for human whole blood containing heparin after 120 min on β-MPAc-Pt formed from 50 alternate soaking cycles. There was no clotting on β-MPAc-Pt. When prota-

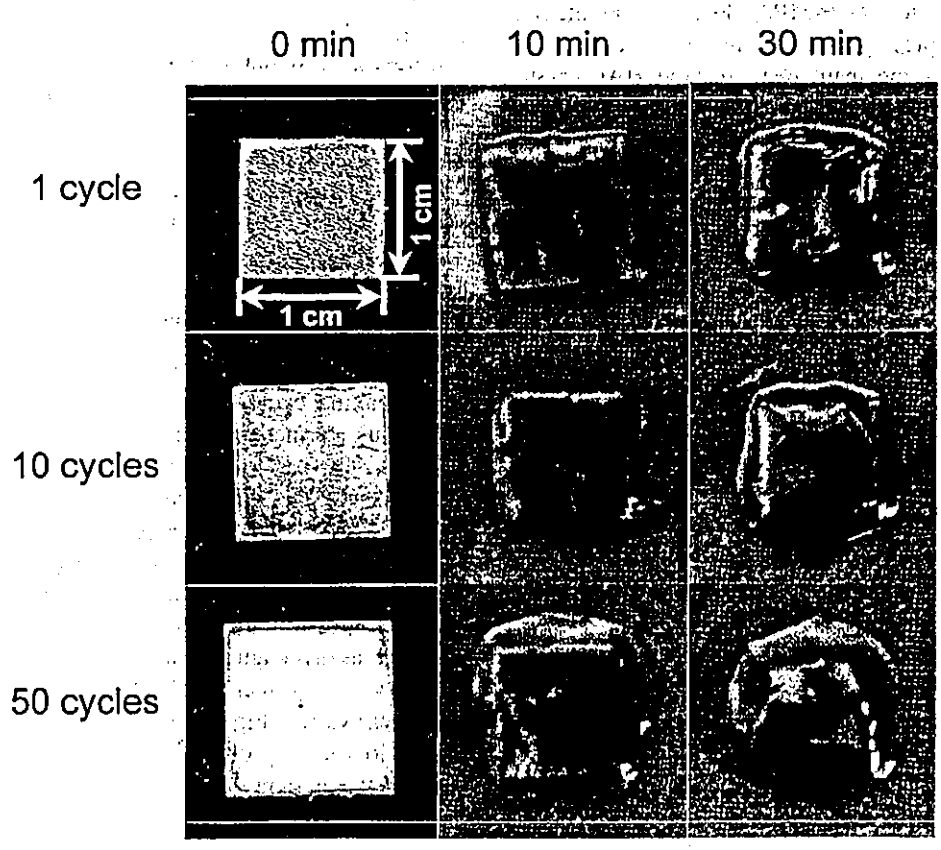

Figure 11. Thrombus formation on the β-MPAc-Pt with HAp after each alternate soaking cycle (1 cycle, 10 cycles and 50 cycles). Thrombus formation at 0, 10, and 30 min after immersion in blood was evaluated.

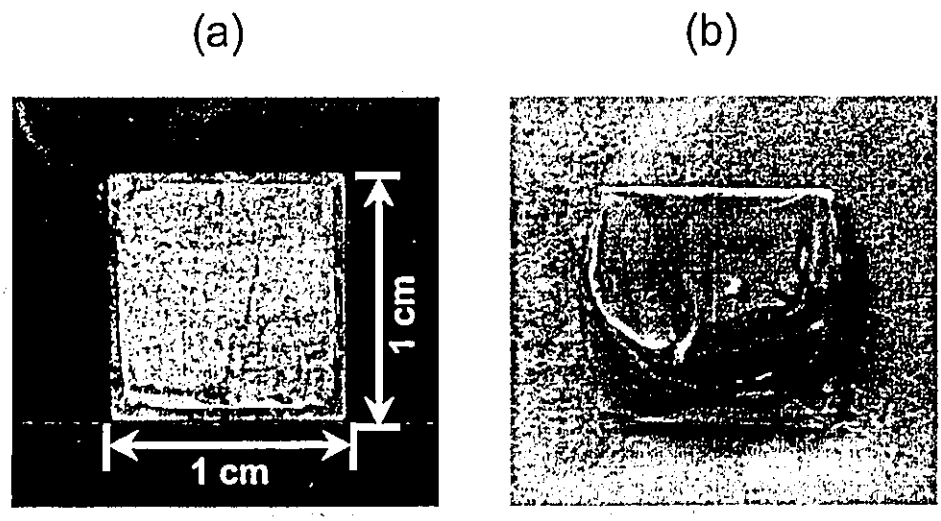

Figure 12. Results of the clotting test for human whole blood containing heparin after 120 min on β-MPAc-Pt formed from 50 alternate soaking cycles (a). Protamine sulfate was added at the appropriate concentration to human whole blood containing heparin. Thrombus formation was then observed after 20 min (b). Protamine sulfate was used in order to inhibit the heparin activity.

mine sulfate was added at the appropriate concentration to human whole blood containing heparin, thrombus formation was observed after 20 min [Figure 12(b)]. If a thrombus is formed in human blood containing heparin during the operation, there is a risk of embolization of the thrombus and detachment from the GDCs due to blood flow. These results suggest that the coagulant activity of HAp can be blocked by heparin. In other words, unheralded embolization is guaranteed by the standard procedure of controlling the clotting time.

The results of this study suggests the possibility of aneurysmal embolization acceleration due to HAp coating on the surface of the GDCs. Furthermore, these results also suggest that HAp-coated β-MPAc-Pt can be used for long term in the aneurysm because when HAp-coated β-MPAc-Pt is put in the aneurysm, a blood clot will immediately form on the surface of HAp layer. The HAp layer will form a blood clot in the aneurysm, reduce recanalization, and enhance tissue regeneration. To accelerate tissue formation, the use of cytokines is an attractive next step. Tamatani et al. and Mcguire et al. reported that the proliferation of endothelial cells was greater on type I collagen than on other ECM proteins such as fibronectin, laminin, or gelatin.[25,26] It is expected that the induction of fibroblast or endothelial cells can be accelerated by basic fibroblast growth factor (bFGF), vascular endothelial growth factor (VEGF), and collagen type I incorporated onto the HAp-coated GDCs surface. Evaluation and further long-term *in vivo* study are ongoing.

The authors would like to acknowledge Dr. T. Serizawa and Dr. Y. Maeda (Kagoshima University, Japan) for their technical support.

REFERENCES

1. Guglielmi G, Vinuela F, Sepetka I. Electrothrombosis of saccular aneurysms via endovascular approach. Part 1: Electrochemical basis, technique, and experimental results. J Neurosurg 1991;75:1–7.
2. Guglielmi G, Vinuela F, Dion J. Electrothrombosis of saccular aneurysms via endovascular approach. Part 2: Preliminary clinical experience. J Neurosurg 1991;75:8–14.
3. Guglielmi G, Vinuela F, Duckwiler G, Dion J, Lylyk P, Berenstein A, Strother C, Graves V, Halbach V, Nichols D, Hopkins N, Ferguson R, Sepetka I. Endovascular treatment of posterior circulation aneurysms by electrothrombosis using electrically detachable coils. J Neurosurg 1992;77:515–524.
4. Richling B, Gruber A, Bavinzski G, Killer M. GDC-system embolization for brain aneurysms—location and follow up. Acta Neurochir 1995;134:177–183.
5. Zubillaga AF, Guglielmi G, Vinuela F, Duckwiler GR. Endovascular occlusion of intracranial aneurysms with electrically detachable coils: Correlation of aneurysm neck size and treatment results. AJNR Am J Neuroradiol 1994;15:815–820.
6. Ahuja AA, Hergenrother RW, Strother CM, Rappe AA, Cooper SL, Graves VB. Platinum coil coatings to increase thrombogenicity: A preliminary study in rabbits. AJNR Am J Neuroradiol 1993;14:794–798.
7. Dawson RC, Krisht AF, Barrow DL, Joseph GJ, Shengelaia GG, Bonner G. Treatment of experimental aneurysms using collagen-coated microcoils. Neurosurgery 1995;36:133–140.
8. Kalmes DF et al. *In vitro* proliferation and adhesion of basic fibroblast growth factor-producing fibroblasts on platinum coils. Radiology 1998;206:237–243.
9. Murayama Y, Vinuela F, Suzuki Y, Akiba Y, Ulihoa A, Duckwiler GR, Gobin YP, Vinters HV, Iwaki M, Abe T. Development of the biologically active guglielmi detachable coil for the treatment of cerebral aneurysms. Part II: An experimental study in a swine aneurysm model. AJNR Am J Neuroradiol 1999;20:1992–1999.
10. Kevor ST, Roger IM, Maria K, Paul WB. Formation and properties of a synthetic bone composite: Hydroxyapatite–collagen. J Biomed Mater Res 1995;29:803–810.
11. Sato K, Kumagai Y, Tanaka J. Apatite formation on organic monolayers in simulated body environment. J Biomed Mater Res 1999;50:16–20.
12. Downes S, Clifford CJ, Scotchford C, Klein CPAT. Comparison of the release of growth hormone from hydroxyapatite, heat-